Epigenetic profiling identifies markers of endocrine resistance and therapeutic options for metastatic castration-resistant prostate cancer

Severson, Tesa M.; Minnee, Emma; Zhu, Yanyun; Schuurman, Karianne; Nguyen, Holly M.; Brown, Lisha G.; Wessels, Lodewyk; Zwart, Wilbert; Bergman, Andries M.; More Authors

DOI
10.1016/j.xcrm.2025.102215

Publication date
2025

Document Version
Final published version

Published in
Cell Reports Medicine

Cell Reports
Medicine

Article

Epigenetic profiling identifies markers of endocrine resistance and therapeutic options for metastatic castration-resistant prostate cancer

Graphical abstract

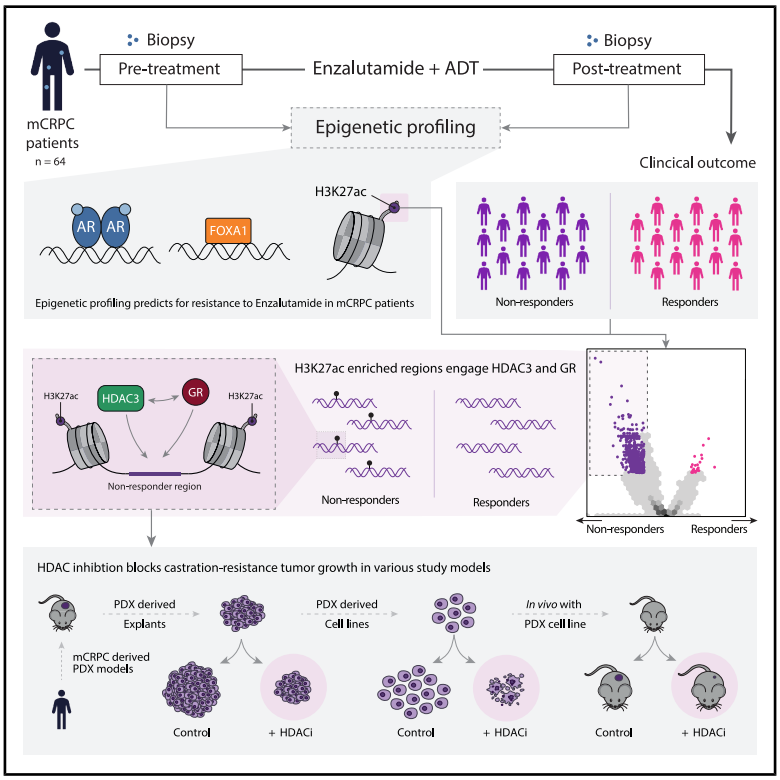

Highlights

- Enhancer profiling predicts resistance to AR inhibition in mCRPC
- Resistance-enriched active enhancers engage HDAC3 and GR
- HDAC inhibition blocks castrate-resistant tumor growth

Authors

Tesa M. Severson, Emma Minnee, Yanyun Zhu, ..., Stefan Prekovic, Wilbert Zwart, Andries M. Bergman

Correspondence

w.zwart@nki.nl (W.Z.), a.bergman@nki.nl (A.M.B.)

In brief

Severson and Minnee et al. identify, in the tumor tissue of patients with metastatic prostate cancer, a distinct genetic program that predicts therapy resistance. Targeting proteins that act through these regions effectively blocks tumor growth and may provide a novel therapeutic strategy for metastatic patients after hormonal therapy resistance develops.

Severson et al., 2025, Cell Reports Medicine 6, 102215
July 15, 2025
https://doi.org/10.1016/j.xcrm.2025.102215

CellPress

Cell Reports Medicine

CellPress
OPEN ACCESS

Article

Epigenetic profiling identifies markers of endocrine resistance and therapeutic options for metastatic castration-resistant prostate cancer

Tesa M. Severson,[1,2,3,24] Emma Minnee,[1,2,24] Yanyun Zhu,[1,2] Karianne Schuurman,[1] Holly M. Nguyen,[4] Lisha G. Brown,[4] Sini Hakkola,[5] Renee Menezes,[6] Sebastian Gregoricchio,[1,2] Yongsoo Kim,[1,21] Jeroen Kneppers,[1,2] Simon Linder,[1,2] Suzan Stelloo,[1,2,22] Cor Lieftink,[7] Michiel S. van der Heijden,[3,8] Matti Nykter,[5] Vincent van der Noort,[9]

(Author list continued on next page)

[1]Division of Oncogenomics, The Netherlands Cancer Institute, 1066 CX Amsterdam, the Netherlands
[2]Cancer Genomics Netherlands, Oncode Institute, 3584 CG Utrecht, the Netherlands
[3]Division of Molecular Carcinogenesis, The Netherlands Cancer Institute, 1066 CX Amsterdam, the Netherlands
[4]Department of Urology, University of Washington, Seattle, WA 98195, USA
[5]Prostate Cancer Research Center, Faculty of Medicine and Health Technology, Tampere University and Tays Cancer Centre, 33100 Tampere, Finland
[6]Biostatistics Centre & Department of Psychosocial Research and Epidemiology, the Netherlands Cancer Institute, 1066 CX Amsterdam, the Netherlands
[7]Division of Molecular Carcinogenesis and NKI Robotics and Screening Center, The Netherlands Cancer Institute, 1066 CX Amsterdam, the Netherlands

(Affiliations continued on next page)

SUMMARY

Androgen receptor (AR) signaling inhibitors, including enzalutamide, are treatment options for patients with metastatic castration-resistant prostate cancer (mCRPC), but resistance inevitably develops. Using metastatic samples from a prospective phase 2 clinical trial, we epigenetically profile enhancer/promoter activities with acetylation of lysine residue 27 on histone 3 (H3K27ac) chromatin immunoprecipitation followed by sequencing, before and after AR-targeted therapy. We identify a distinct subset of H3K27ac-differentially marked regions that are associated with treatment responsiveness, which we successfully validate in mCRPC patient-derived xenograft (PDX) models. *In silico* analyses reveal histone deacetylase (HDAC)3 to critically drive resistance to hormonal interventions, which we validate *in vitro*. Critically, we identify the pan-HDAC inhibitor vorinostat to be effective in decreasing tumor cell proliferation, both *in vitro* and *in vivo*. Moreover, we uncover evidence for HDAC3 working together with glucocorticoid receptor (GR) as a potential mechanism for this therapeutic effect. These findings demonstrate the rationale for therapeutic strategies including HDAC inhibitors to improve patient outcome in advanced stages of mCRPC.

INTRODUCTION

Prostate cancer is the most prevalent cancer type in men, with globally over 1.4 million new diagnoses and 396,000 patients who succumb to the disease each year.[1] Although most patients with high-risk localized disease are effectively treated with prostatectomy or radiotherapy,[2] eventually 25% of patients will develop metastases for which there is currently no cure.[3–5] The treatment of choice for patients with metastatic prostate cancer is androgen deprivation therapy (ADT), which reduces serum testosterone to castration levels, to which virtually all patients initially respond. However, metastatic disease progression despite ongoing ADT, termed metastatic castration-resistant prostate cancer (mCRPC), is inevitable.[6]

Androgen receptor (AR) is a hormone-dependent transcription factor and the master regulator of prostate cancer development and progression. Upon androgen stimulation, AR translocates into the nucleus[7] and associates with distal regulatory elements throughout the genome, hereafter referred to as its "cistrome."[8,9] AR chromatin binding is facilitated by pioneer factors, such as FOXA1,[10] and operates under tight epigenetic control.[10,11] Most active AR sites are hallmarked by acetylation of lysine residue 27 on histone 3 (H3K27ac), a marker of active enhancers and promoters.[12,13] Upon formation of an active transcription complex, AR drives the expression of its target genes to control tumor cell growth. Following progression on ADT, further suppression of the AR signaling axis by inhibitors such as enzalutamide (ENZA) is an effective treatment for patients with mCRPC.[14,15]

Joyce Sanders,[10] Ben Morris,[7] Guido Jenster,[11] Geert JLH van Leenders,[12] Mark Pomerantz,[13] Matthew L. Freedman,[13,14] Roderick L. Beijersbergen,[7] Alfonso Urbanucci,[5,15] Lodewyk Wessels,[2,3,16] Peter S. Nelson,[17,18] Eva Corey,[4] Stefan Prekovic,[1,2,23] Wilbert Zwart,[1,2,19,*] and Andries M. Bergman[1,8,20,25,*]

[8]Division of Medical Oncology, The Netherlands Cancer Institute, 1066 CX Amsterdam, the Netherlands
[9]Department of Biometrics, The Netherlands Cancer Institute, 1066 CX Amsterdam, the Netherlands
[10]Department of Pathology, The Netherlands Cancer Institute, 1066 CX Amsterdam, the Netherlands
[11]Department of Urology, Erasmus MC, 3015 GD Rotterdam, the Netherlands
[12]Department of Pathology, Erasmus MC Cancer Institute, 3015 CP Rotterdam, the Netherlands
[13]Department of Medical Oncology, Dana-Farber Cancer Institute, Harvard Medical School, Boston, MA 02215, USA
[14]The Eli and Edythe L. Broad Institute, Cambridge, MA 02142, USA
[15]Department of Tumor Biology, Institute for Cancer Research, Oslo University Hospital, 0424 Oslo, Norway
[16]Department of EEMCS, Delft University of Technology, 2628 CM Delft, the Netherlands
[17]Divisions of Human Biology and Clinical Research, Fred Hutchinson Cancer Center, Seattle, WA 98109, USA
[18]Department of Medicine, Division of Medical Oncology, University of Washington, Seattle, WA 98195, USA
[19]Laboratory of Chemical Biology and Institute for Complex Molecular Systems, Department of Biomedical Engineering, Eindhoven University of Technology, 5600 MB Eindhoven, the Netherlands
[20]Department of Medical Oncology, Amsterdam UMC, University of Amsterdam, 1105 AZ Amsterdam, the Netherlands
[21]Present address: Department of Pathology, Amsterdam University Medical Center, Cancer Center Amsterdam, 1081 HV Amsterdam, the Netherlands
[22]Present address: Department of Molecular Biology, Faculty of Science, Radboud Institute for Molecular Life Sciences, Radboud University, Nijmegen, 6525 GA Nijmegen, the Netherlands
[23]Present address: Center for Molecular Medicine, University Medical Center Utrecht, 3584 CX Utrecht, the Netherlands
[24]These authors contributed equally
[25]Lead contact
*Correspondence: w.zwart@nki.nl (W.Z.), a.bergman@nki.nl (A.M.B.)
https://doi.org/10.1016/j.xcrm.2025.102215

ENZA is a well-established therapy for the treatment of mCRPC. It significantly decreases the risk of radiographic progression and death in both the pre- and post-chemotherapy settings.[14,15] ENZA blocks AR signaling at multiple levels, including diminished AR chromatin binding and prevention of coregulator recruitment.[16] However, intrinsic resistance to ENZA is observed in up to 46% of patients with mCRPC, and the duration of response varies greatly between patients.[14,15] Consequently, biomarkers for response prediction to AR-targeted therapeutics, including ENZA, are urgently needed to identify those patients who may benefit from alternative treatment strategies. Moreover, combination treatments to overcome or postpone resistance to AR-targeted therapies are urgently needed in the clinic.

Several studies compared AR chromatin binding profiles in different disease stages and illustrated the plasticity of AR cistromes in tumor development[8,17] and disease progression,[18,19] which are predictive for outcome[19] and associated with treatment response in cell lines.[11] However, there is limited knowledge on FOXA1 cistromics and H3K27ac profiles, in relation to drug resistance in patients with mCRPC.

To identify the potential epigenetic alterations that drive ENZA response in patients with mCRPC, metastasis-targeted biopsies were collected pre- and post AR-targeting treatment, while response to treatment was monitored. Comparative cistromic analyses revealed a specific subset of 657 H3K27ac sites significantly enriched in metastatic lesions from patients with mCRPC who did not respond to AR-targeted treatment. These sites were associated with lack of response to castration in mCRPC patient-derived xenograft (PDX) models and regulate genes selectively expressed in ENZA-resistant cell line models, illustrating their potential to predict treatment response. Finally, we identified and functionally assessed factors that selectively bind to these 657 resistance-associated H3K27ac sites in cell line models, revealing therapeutic candidates and a potential effective treatment strategy for patients with ENZA-resistant mCRPC. Furthermore, we propose a role for glucocorticoid receptor (GR) acting in combination with histone deacetylase (HDAC)3 at ENZA resistance-associated enhancer regions, to drive resistance to ENZA.

RESULTS

Phase 2 trial of AR-targeted therapy in patients with mCRPC

To identify epigenetic biomarkers, we conducted a single-arm, open-label, phase 2 study in patients with mCRPC treated with a new line of AR-targeted therapy, as a sub-investigation of the CPCT-02 biopsy protocol (NCT01855477) (Figure 1A). Between September 2014 and April 2019, a total of 64 patients with mCRPC were enrolled in the trial. Baseline characteristics are summarized in Table S1, and trial outcomes in Table S1 and Figure S1A. In-depth description of relevant clinicopathological parameters and outcomes is included in the STAR Methods.

Biopsy assessment and evaluable population for biomarker discovery

All 64 patients had a pre-treatment biopsy from a metastatic lesion. Biopsy sites include bone (n = 19; 29.7%), lymph nodes (n = 32; 50.0%) and visceral organs (n = 13; 20.3%) (Table S1). A second biopsy (post-treatment) was taken upon disease progression for 15 patients. Biopsies with $\geq$30% tumor cells were further processed for downstream molecular analyses (42 and 12 for pre- and post-treatment, respectively) (Figure S1A). None of the patients who had post-treatment biopsies were treated with ENZA at the time of biopsy. We successfully

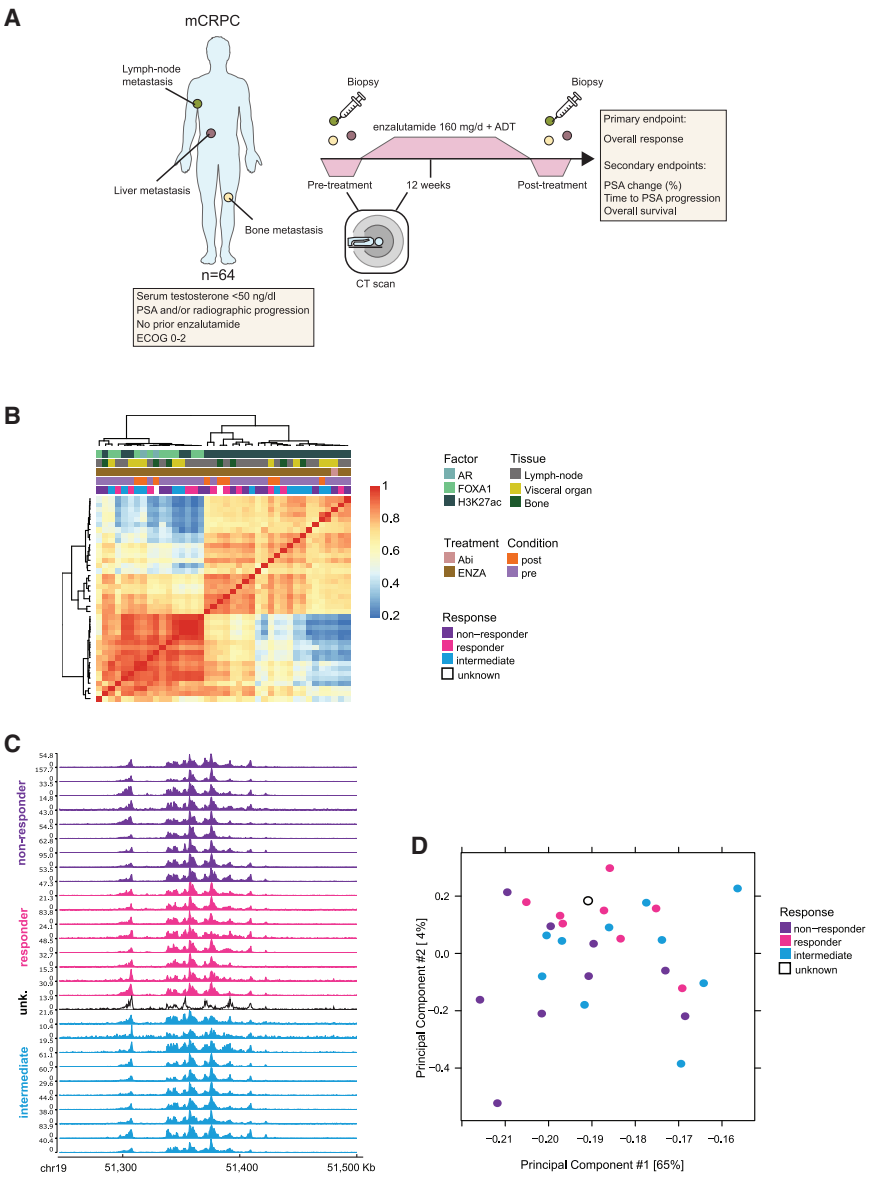

Figure 1. Clinical trial design and ChIP-seq data collection

(A) Setup of the clinical trial. Patients with mCRPC are enrolled in the study, and an imaging-guided biopsy is taken prior to onset of ENZA treatment. One patient in the study was treated with abiraterone.

(B) Correlation heatmap of ChIP-seq data (50 kb bins across the genome, Pearson correlation) for H3K27ac, AR, and FOXA1 among all mCRPC samples (n = 40). Colors bars indicate ChIP factors: AR (light blue), FOXA1 (light green), and H3K27ac (dark green); tissue of sample origin: lymph node (gray), visceral organ (yellow), and bone (dark green); treatment: abiraterone (Abi, salmon) and enzalutamide (ENZA, brown); condition of the sample: pre-treatment (purple) and post-treatment (orange); and treatment response: non-responder (dark purple), responder (pink), intermediate (blue), and unknown (black outline). Scale bar indicates low (blue) to high correlation (red).

(C) Snapshot of H3K27ac ChIP-seq (biological replicates, n = 28) in different treatment response groups: responders (pink), non-responders (purple), unknown (unk., black outline), and intermediate (blue). The read counts (left) and genomic coordinates (bottom) are indicated.

(D) Principal component analysis using normalized read counts in all peaks in H3K27ac ChIP-seq data (n = 73039) from all samples (biological replicates, n = 28). Samples labeled according to responders (pink), non-responders (purple), intermediate (blue), or unknown (white).

See also Figure S1; Tables S1 and S2.

generated chromatin immunoprecipitation sequencing (ChIP-seq) data for active promoter/enhancer histone modification H3K27ac—passing stringent quality control (QC) requirements (see STAR Methods)—for 22 out of the 42 samples. Four (18.2%) of the evaluable pre-treatment biopsies were from bone metastases, 13 (59.1%) from lymph node metastases, and 5 (22.7%) from visceral metastases (Table S1). For 6 of 15 post-treatment biopsies, we obtained high-quality H3K27ac ChIP-seq data: 1 (16.7%) from bone, 3 (50.0%) from lymph nodes, and 2 (33.3%) from visceral organs. One patient had both pre- and post-treatment biopsies, resulting in 28 biopsy samples for further analyses from 27 unique patients. The baseline characteristics and treatment outcomes of the patients who donated an evaluable pre-treatment (n = 22) or post-treatment (n = 6) biopsy are summarized in Table S1. There were no significant differences in baseline age, serum prostate-specific antigen (PSA), treatment outcomes, duration of treatment, PSA change from baseline, and time to PSA progression (TTPP) between the patients who donated an evaluable pre- and/or post-treatment biopsy and the whole population (Table S1). Survival data are also included in Table S1.

All patients were categorized based on overall response, which was a composite of three outcomes: (1) $\geq$ 50% PSA decrease from baseline, (2) radiographic response (stable disease, partial response, or complete response), and (3) longer than median TTPP. Assessment was conservative; in case a patient could not be evaluated on a particular outcome measure, it was considered as no response. All patients were evaluable, except for one patient (1.6%) who could not be evaluated for any of the three outcomes (Table S1). In the whole population, 23.4% of patients scored on all three items (response to ENZA), 37.5% of patients did not score on any item (no response to ENZA), and the remaining 37.5% of patients had inconsistent responses on the three outcome measures listed earlier (intermediate response to ENZA). Of the 22 patients in the pre-treatment evaluable population, 6 (27.3%) patients had a response, 8 (36.4%) had an intermediate response, and 8 (36.4%) had no response to ENZA (Table S1). Of the 6 patients in the post-treatment evaluable

population, 2 patients had a response (33.3%), 2 had an intermediate response (33.3%), and 1 patient had no response (16.7%) to ENZA treatment, while 1 patient was not evaluable (16.7%) (Table S1). Based on the ChIP-seq QC parameters and clinical assessment of our trial data, 28 biopsies (22 pre- and 6 post-treatment, from 27 unique patients) with high-quality ChIP-seq data are available; roughly equally sized response groups were formed, with 8 responders, 10 intermediate responders, and 9 non-responders to treatment (one unknown) (Figure 1B).

Genome-wide epigenetic profiling of mCRPC

Apart from H3K27ac ChIP-seq data, for which we successfully generated high-quality data for 28 metastatic biopsy samples (see the previous section), 10 FOXA1 ChIP-seq and 2 AR ChIP-seq datasets were generated (Figures 1B and S1A). As all these patients received prior ADT, the low circulating testosterone levels may explain the relatively low success rate of AR ChIP-seq (in which chromatin binding is decreased following ADT) as compared to FOXA1. For peak numbers, read counts, and other relevant ChIP-seq QC parameters, see Table S2 and Figures S1B and S1C.

H3K27ac ChIP-seq samples were highly correlated based on genome-wide patterns (Figure 1B) indicating low inter-tumor heterogeneity and robust technical reproducibility. As expected, and in line with our previous study on multiple metastases from the same patient,[20] FOXA1 and AR profiles were intermingled in our unsupervised hierarchical analysis, reflecting the direct biological interplay between these two factors.[8,21] No correlation was observed with metastatic site, treatment condition/status, or clinical response in the clustering with all factors (Figure 1B), nor in clustering on H3K27ac alone (Figures S1D and S1E). As H3K27ac ChIP-seq data represented the largest and most complete dataset, we decided to focus on these samples. For H3K27ac profiles, we found comparably high-quality peaks across all three response groups, as exemplified at a single locus (Figure 1C; AR and FOXA1, Figure S1F) and on a genome-wide scale (Figure 1D).

Distinct H3K27ac profiles identify mCRPC tumors resistant to AR-targeted therapy

When taking all peaks in all samples into account, H3K27ac profiles did not differ between response groups of patients in an unsupervised exploratory analysis (principal component analysis) showing the most variance in the data (Figure 1D). To identify subsets of regions that may stratify patients on outcome, we performed supervised differential binding analysis[22] on H3K27ac data, comparing responders and non-responders (Figure 2A). In total, we observed 682 H3K27ac regions that significantly differed between these response groups, with 657 sites selectively enriched in non-responder patients and merely 25 sites found selectively enriched in responders (false discovery rate [FDR]-adjusted p value ≤ 0.05, $\log_2$FC $\geq$ abs|2|, Figure 2B). As expected for H3K27ac ChIP-seq, both sets of sites are predominantly found in distal intergenic regions (Table S2). Differentially enriched peaks between responders and non-responders were robust, as exemplified for three genomic loci (Figure 2C), and quantified showing enriched signal in non-responders compared to responders across all non-responder sites (Figure 2D). The non-responder enriched sites are associated with super-enhancers identified in the prostate cancer cell line derived from lymph-node, LNCaP (Fisher's exact test, p value < 0.0001)[23] indicating their potential importance for controlling cell state. Associated genes (Table S3, genes with TSS within 50 kb of non-responder H3K27ac peak) were significantly enriched for non-canonical AR target genes[24] (hypergeometric test, p value < 0.0001), indicating the potential non-canonical AR function in therapy-targeted resistance. Genes associated with non-responder sites previously implicated in aggressive prostate cancer, PCAT1[25] and WNT5A[26] (Table S3), show higher H3K27ac signal in non-responder samples (Figure S1G).

To determine whether the 657 H3K27ac non-responder sites represent an acquired feature of mCRPC, or whether H3K27ac signal at these regions is already present in the primary disease setting and associated with aggressiveness, we re-analyzed H3K27ac ChIP-seq data from a matched case-control cohort of patients with treatment-naive primary prostate cancer that we reported previously.[9] We observed no difference in H3K27ac signal at these sites based on case/control status (Figure S4A), nor on Gleason score (7 versus 9) (Figures S1H and S1I) while typical signal for known primary-specific AR-binding sites was clearly present[8] (Figure S1J). Further supporting the notion that these regions are acquired in the treatment resistance metastatic setting, we observed stronger signal in the non-responder metastatic samples (this study) compared with treatment-naive metastasis samples and previously reported primary prostate cancer samples[18] as well as healthy prostate tissue[18] (Figure S1K).

Resistance-associated H3K27ac profiles predict response to castration in mCRPC PDXs

To independently validate the stratification potential of our resistance-associated H3K27ac sites beyond our current mCRPC patient samples, we next investigated an existing H3K27ac ChIP-seq dataset that we previously reported for mCRPC PDX models.[18] The PDX models were generated from castration-resistant prostate cancer tumors and represent metastatic samples from multiple metastatic sites, including adrenal glands, ascites, bladder, bone, bowel, lymph node, and liver.[27] Originally, to determine the hormone dependency of PDX tumor growth, PDX tumors were grown in testosterone-proficient male mice, after which the animals were either castrated or left intact (see overview in Figure 3A).

To evaluate whether the PDX tumors could be discriminated based upon the 657 non-responder H3K27ac sites, we plotted H3K27ac ChIP-seq data for these sites in 15 available LuCaP PDX samples derived from tumors from patients with prostate cancer (Figures 3B and 3C). Interestingly, 7 PDXs (45%) displayed strong H3K27ac signal at these regions, while the remaining 8 PDX samples (55%) displayed weak signal at these sites (assessed visually, Figure 3B), with no significant global differences between these two groups of samples (Figure S2A). Integrating these cistromic data with *in vivo* response-to-castration data showed that PDXs with strong H3K27ac at our clinically observed non-responder sites responded less to castration (Figure 3D; raw data, Figure S2B), relative to PDXs with weak H3K27ac signal at these sites. We used cell line models derived from a PDX (cPDX) with strong

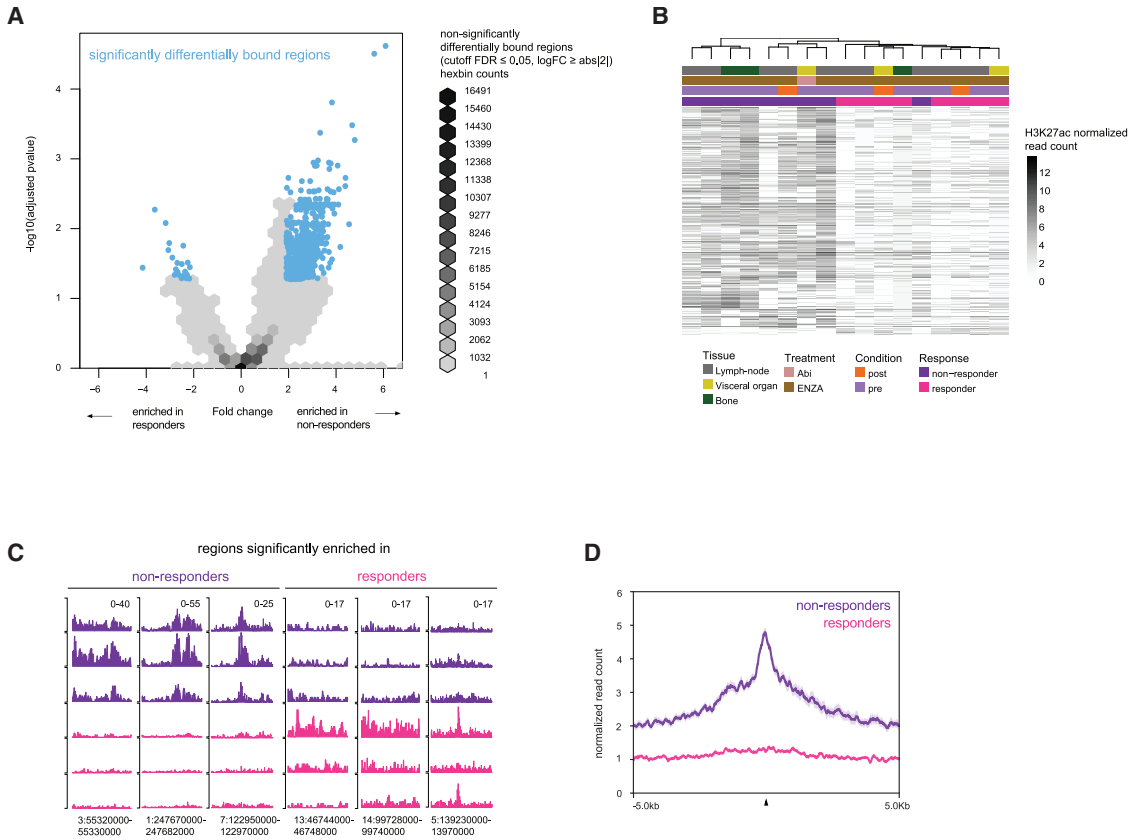

Figure 2. Distinct H3K27ac profiles stratify patients with mCRPC on response to AR inhibition

(A) Differentially enriched regions from H3K27ac ChIP-seq data visualized by volcano plot (n = 73,039). Regions marked by blue dots were significant (DiffBind DESeq2 two-tailed FDR-adjusted p value $\leq$ 0.05, $\log_2$FC $\geq$ abs|2|) (n = 848); all other regions are shown with hexbin density to avoid over-plotting (n = 72191). Each data point density tile (hexagon) represents the density of data within the tile from low (light gray) to high (black).

(B) Heatmap showing normalized read count of H3K27ac data in significantly differentially bound regions (DiffBind DESeq2 two-tailed FDR-adjusted p value $\leq$ 0.05, $\log_2$FC $\geq$ abs|2|) (n = 848) in responder (n = 8) and non-responder samples (n = 9), biological replicates. Colors bars indicate tissue of sample origin: lymph node (gray), visceral organ (yellow), and bone (dark green); treatment: abiraterone (Abi, salmon) and enzalutamide (ENZA, brown); condition of the sample: pre-treatment (purple) and post-treatment (orange); and treatment response: non-responder (dark purple) and responder (pink). Scale bar indicates low (white) to high (black) normalized read counts.

(C) Individual snapshot of H3K27ac enriched differently in 3 responder patients (pink) and 3 non-responder patients (purple) as examples (biological replicates). The read counts and genomic coordinates are indicated (top right and bottom, respectively).

(D) Average normalized H3K27ac read count profiles of all merged data for responder patients (pink, n = 8) and all merged non-responder patients (purple, n = 9) at the 657 non-responder enriched sites (±5 kb from the peak center). Shading indicates standard error of the data.

See also Figure S1; Table S2.

H3K27ac (LuCaP 189.4) or weak (LuCaP 35) signal at our 657 resistance-associated sites, as surrogates for non-responder/responder status, to delve into the mechanistic properties of response.[27] These cPDXs express comparable levels of AR, FOXA1, and H3K27ac as determined by western blot (Figure 3E) and recapitulate H3K27ac, AR, and FOXA1 signals of the non-responder and responder patient samples (Figure 3E), further supporting their role as suitable models for response in this setting. We found, upon stimulation, no change in expression of genes associated with non-responder H3K27ac peaks (TSS within 50 kb of a peak, Table S3) (Figure S2C). Interestingly, using single-cell RNA sequencing data (scRNA-seq) from prostate cancer cell lines, we do find genes associated with our clinically observed H3K27ac non-responder sites as significantly enriched in a cell cluster that selectively appears in LNCaP-derived ENZA-resistant cells[28] (cluster 3) (Figure 3F; Table S2). Further supporting these findings, when analyzing scATAC-seq (single-cell assay for transposase-accessible chromatin using sequencing) data from the same cells, we identified overlap of our non-responder H3K27ac peaks with accessible regions in the ENZA-resistant cluster 3 (Table S2), cumulatively suggesting potential clonality of resistant cells toward this specific cell population. After long-term treatment with ENZA, cluster 3 was enriched mainly for LNCaP RES-B-resistant cells and partially for RES-A cells. LNCaP RES-B cell cluster 3 was expanded relative to parental cells as well as RES-A, indicating that these cells drive resistance-specific biology. In addition, average expression of genes associated with H3K27ac non-responder sites was linked with cluster 3 expansion (Figure 3G). Given the metastatic nature of LNCaP and its ENZA-resistant

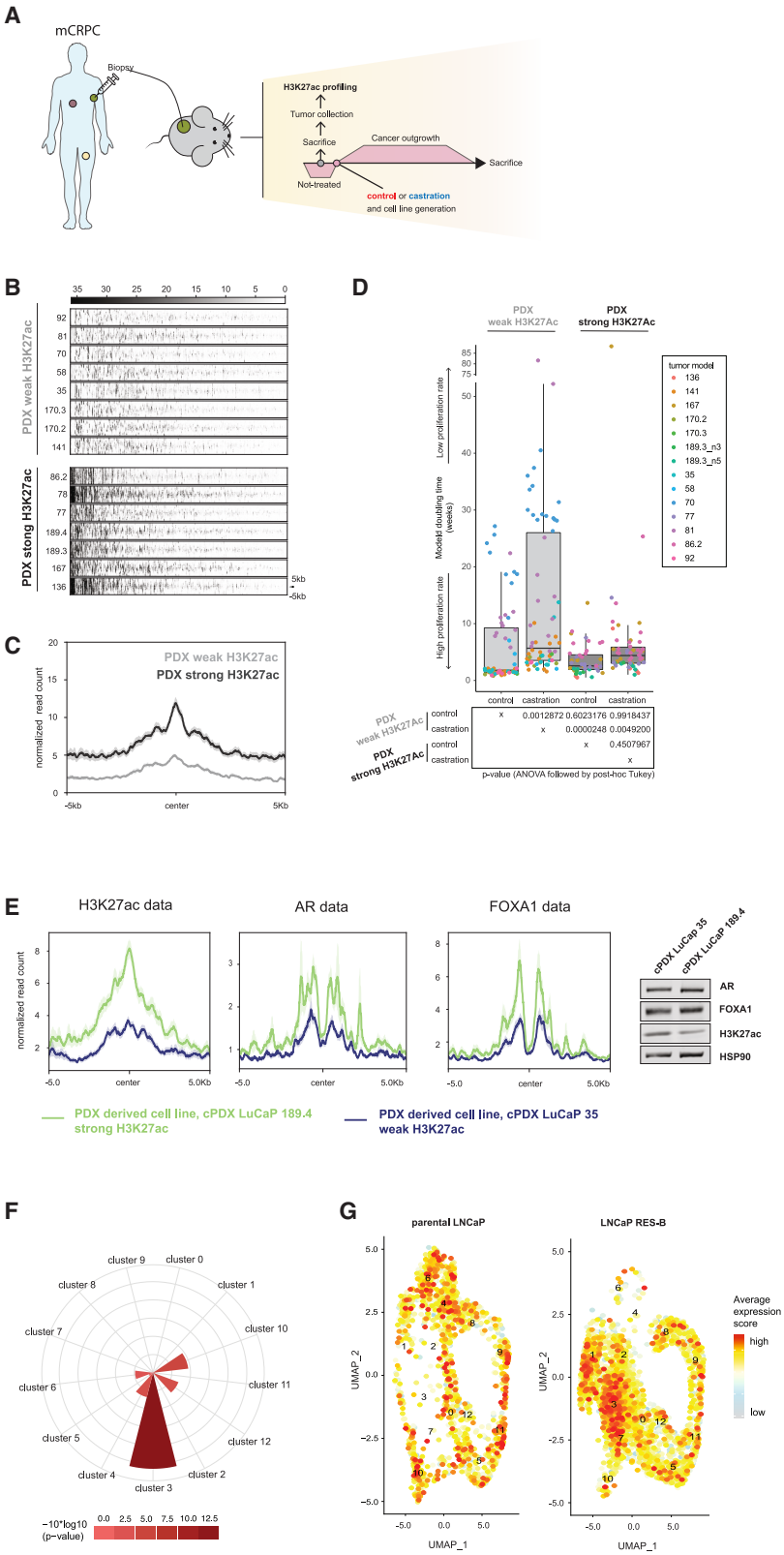

Figure 3. mCRPC PDX, PDX-derived cell line, and scRNA-seq validations of resistance-associated H2K27ac regions

(A) Overview of the PDX models setup. Prostate cancer samples from patients with mCRPC were obtained and implanted into the mouse to establish PDXs. These PDXs were characterized previously with their response to castration by the change of tumor volume.

(B) Heatmap depicting raw read counts of H3K27ac ChIP-seq signal from PDX samples at the non-responder-enriched 657 H3K27ac regions, identified from the mCRPC patient samples (±5 kb from the peak center). Scale bar indicates low (white) to high (black) read counts.

(C) Average normalized H3K27ac read count profiles of all PDX merged data for samples with weak (gray, n = 8) and strong (black, n = 7) signal in the non-responder 657 H3K27ac regions (±5 kb from the peak center), biological replicates. Shading indicates standard error of the data.

(D) Boxplots depicting doubling time of PDX models estimated using exponential (Malthusian) growth model (y axis) by group (x axis). The central mark indicates the median, and the bottom and top edges of the box indicate the 25th and 75th percentiles, respectively. The maximum whisker lengths are specified as 1.5 times the interquartile range. All individual values are depicted as circles colored by PDX model (strong H3K27ac – castration: n = 57, strong H3K27ac – control: n = 45, weak H3K27ac – castration: n = 71, weak H3K27ac – control: n = 73, biological replicates). Table below indicates the p values obtained for one-way ANOVA followed by Tukey honest significant difference (HSD) test for all combinations.

(E) (Left) Average normalized H3K27ac read count profiles of all cPDX cell line merged data for non-responder classed sample, cPDX LuCaP 189.4 (green, n = 3) and responder classed sample, cPDX LuCaP 35 (dark blue, n = 3) signal in the non-responder 657 H3K27ac regions (±5 kb from the peak center), biological replicates. Shading indicates standard error of the data. (Middle) Same as above with AR data. (Right) Same as above with FOXA1 data. (Far right) Western blot of AR, FOXA1, H3K27ac, and HSP90 (control) for cPDX LuCaP 35 and cPDX LuCaP 189.4. Shading indicates standard error of the data.

(F) Polar plot reporting the $-10 \times \log_{10}(p$ values) (Fisher's exact test) of gene overlap enrichment tests between genes associated with H3K27ac non-responder regions and LNCaP scRNA-seq cluster marker genes. Color indicates strength of significance from low (pink) to high (red).

(G) Uniform manifold approximation and projection (UMAP) visualization showing the average gene expression score of genes associated with H3K27ac non-responder regions in the parental LNCaP (left) and the ENZA-resistant, RES-B (right) single cells. Original scRNA-seq clusters (0–12) are superimposed on each plot. Scale bar indicates average expression score from low (gray) to high (red).

See also Figure S2; Table S2.

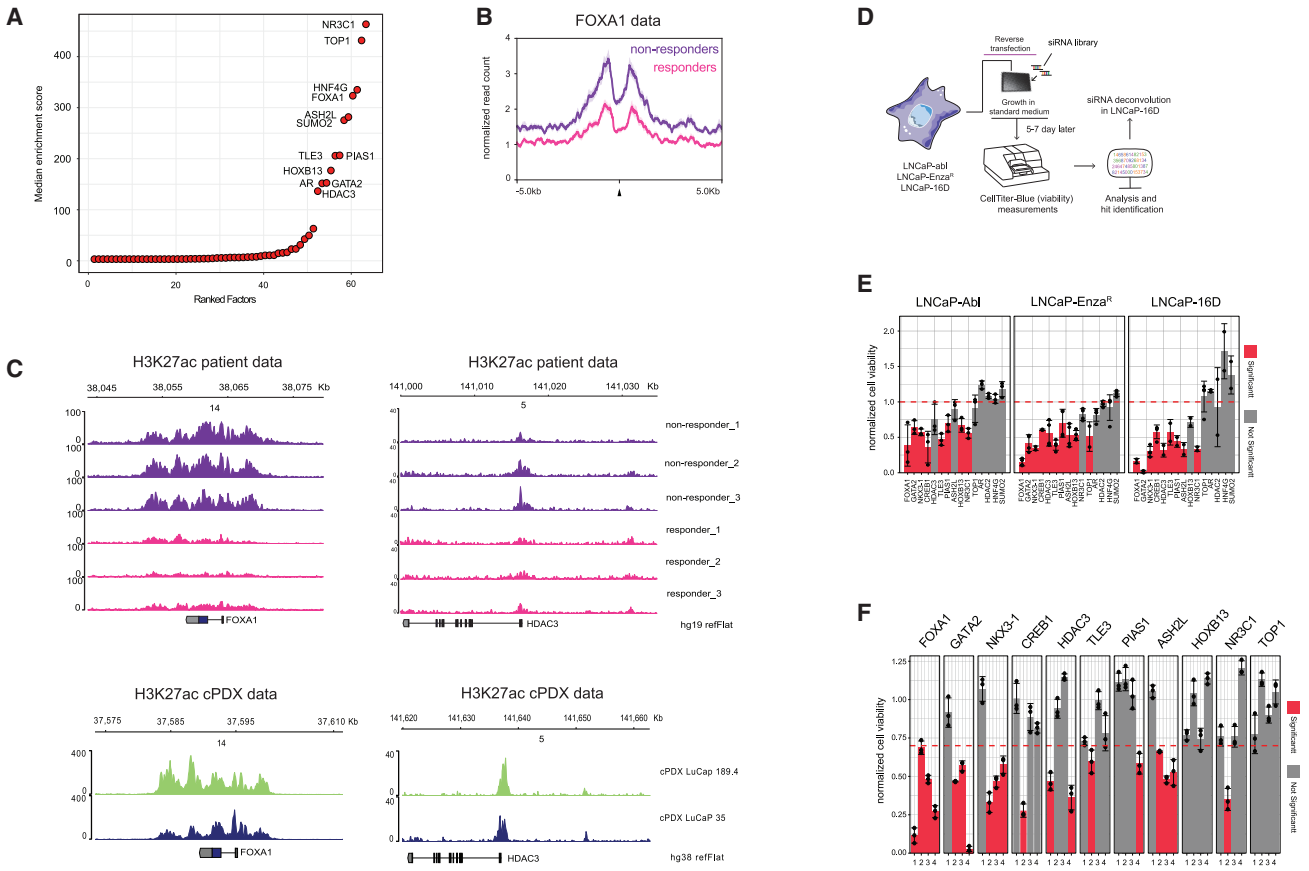

Figure 4. Characterization of the non-responder-enriched H3K27ac sites reveals drivers of resistance

(A) Enrichment analysis to determine significant overlap of 657 H3K27ac non-responder sites with publicly available ChIP-seq data for factors previously studied in prostate cancer cell lines (n = 863). Graph shows median enrichment score for each factor (GIGGLE combo score, indicating low to high significant enrichment score [Fisher's exact two-tailed test and odds ratio]). Factors are ordered by highest score (enrichment) in the dataset with text shown in those with median enrichment score >100.

(B) Average normalized FOXA1 read count profiles of merged data, at the 657 non-responder-enriched H3K27ac sites (±5 kb from the peak center), comparing patient samples, responders (pink, n = 8), and non-responders (purple, n = 9), biological replicates. Shading indicates standard error of the data.

(C) (Left, top) Snapshot of H3K27ac ChIP-seq (3 chosen at random for each class) in different treatment response groups: responders (pink), non-responders (purple) at the FOXA1 locus. The read counts (left) and genomic coordinates (top) are indicated. (Left, bottom) Snapshot of H3K27ac ChIP-seq (one chosen at random for each class) in different treatment response groups from cPDX LuCaPs: responder (dark blue), non-responder (green) at the FOXA1 locus. The read counts (left) and genomic coordinates (top) are indicated. (Right, top) Same as left but for HDAC3 locus. (Right, bottom) Same as left but for HDAC3 locus.

(D) Setup of siRNA screen to identify factors critical of prostate cancer cell line viability, resistant to androgen ablation or ENZA treatment.

(E) Screen results for pooled siRNAs, showing decreased viability of prostate cancer cell line models LNCaP-Abl (left), LNCaP-Enz^R (middle), and LNCaP-16D (right). Cell viability was determined by CellTiter-Blue, and data are normalized over siControl. Bars indicate mean values ±SD ($n \geq 2$, technical replicates). Adjusted p values were determined by two-sided t test with multiple testing correction (Benjamini-Hochberg method). Statistically significant conditions (adjusted p value < 0.05) are shown in red.

(F) siRNA deconvolution experiment, separately analyzing each individual siRNA for the 11 remaining hits in LNCaP-16D cells on cell viability. Cell viability was determined by CellTiter-Blue, and data are normalized over siControl. Bars indicate mean values ±SD ($n \geq 3$, technical replicates). Adjusted p values determined as above. Statistically significant conditions (Benjamini-Hochberg adjusted p values < 0.05) are shown in red.

See also Figures S3 and S4; Table S3.

derivative LNCaP RES-B, confirming our epigenetic results from patients with mCRPC and mCRPC PDX models, we conclude that these datasets represent a clinically relevant model for our analyses. Together, these data illustrate that distinct H3K27ac signals stratify patients for response to AR blockade, which we also observed in mCRPC PDX models, newly developed LuCaP PDX-derived cell lines, and single-cell data from models of ENZA resistance.

Driver identification for resistance to AR inhibition in mCRPC

Using GIGGLE, a genomics search engine that allows for the ranking of significance of genomic loci shared between query (non-responder regions) and a database of ChIP-seq regions,[29] we analyzed an extensive database of ChIP-seq experiments from prostate tissue-derived cell lines and prostate cancer cell lines[30,31] (Table S3) to explore overlap of binding of regions

from DNA-associated proteins with our non-responder H3K27ac sites (Figure 4A). This analysis identified multiple factors previously reported to drive resistance to ENZA or castration, including HNF4G,[32] NR3C1 (GR),[33–35] and FOXA1[36] (Table S3). FOXA1 ChIP-seq analyses from our mCRPC samples revealed selective enrichment at the 657 non-responder H3K27ac sites in mCRPC samples from non-responder patients (n = 4), relative to responders (n = 3) samples, clinically validating the cell line-based GIGGLE analysis (Figure 4B). These results were further confirmed in cPDX cell line data for H3K27ac and FOXA1 (Figure 3E), identifying higher H3K27ac signal at both FOXA1 and HDAC3 genic loci in non-responders (Figure 4C).

Next, we explored the functional involvement of top-enriched factors (Table S3) in driving resistance to AR blockade (essential genes in our setting), by designing and performing a focused small interfering RNA (siRNA) screen of genes with median GIGGLE combo enrichment score >20 to target genes (STAR Methods) in two cell line models of castration resistance (LNCaP-Abl[37] and LNCaP-16D[38]) as well as a model of ENZA resistance (LNCaP-Enz^{R})[39] (Figure 4D). From the pooled siRNA experiments, 11 hits that significantly diminished proliferation (Figure 4E) were identified as top-enriched factors in the GIGGLE analysis and selected for deconvolution experiments in castration-resistant LNCaP-16D. These analyses identified factors previously described as critical in driving resistance to both ENZA and castration in prostate cancer cell lines: FOXA1[36] and GATA2[40] (Figures 4F and S3A). Furthermore, two factors previously associated with castration resistance, but not studied before for their potential involvement in driving resistance to ENZA, were identified: HDAC3[41] and ASH2L.[42]

HDAC inhibition blocks mCRPC cell growth

Computational analyses and perturbation studies identified five factors of potential therapeutic interest. As transcription factors are considered challenging drug targets, we prioritized HDAC3 for further downstream studies. HDAC3 has previously been reported as a therapeutic target in castration-resistant prostate cancer[41] but remains unexplored in the ENZA-resistant setting. While HDAC1, 2, 3, and 8 have been targeted with various HDAC inhibitors, only HDAC3-selective inhibition has been implicated in anti-tumor efficacy in castration resistance.[41] Highly selective HDAC3 inhibitors have been described but have not been explored for efficacy and tolerability in clinical trials.[43] Contrastingly, less-specific HDAC inhibitors are well characterized and clinically implicated in the treatment of several cancer types, including vorinostat in the treatment of cutaneous T cell lymphoma.[44] Vorinostat blocks prostate cancer cell proliferation[41,45] and synergizes with AR antagonist bicalutamide.[46] Consequently, HDAC inhibitors have the potential to overcome resistance to established mCRPC treatments, including AR-targeted drugs.[47] An increased sensitivity to HDAC inhibition was observed in castration-resistant LNCaP-16D cells relative to hormone-sensitive parental LNCaP cells (Figure S3B). Importantly, in both LNCaP cells and LNCaP-16D cells, vorinostat combined with ENZA strongly reduced tumor cell viability (Figure S4A). To further establish therapeutic proof of concept, subcutaneous PDX tumors were dissociated and treated *ex vivo* with increasing concentrations of ENZA, vorinostat, or both (Figures 5A and S4B). In agreement with the cell line-based results, *ex vivo* drug response in mCRPC PDXs confirmed sensitivity to both drugs and synergistic interactions between vorinostat and ENZA in explant experiments (Figures S4A and S4B) using highest-single agent synergy reference model. Through HDAC3 ChIP-seq analyses, we find HDAC3 binding in non-responder H3K27ac regions verifying the GIGGLE analysis (Figure S5A). Furthermore, treatment with the pan-HDAC inhibitor vorinostat increases global and local H3K27ac signal in non-responder regions (Figures S5B and S5C). This increase is higher in comparison to the HDAC3-specific inhibitors, RGFP966 and BRD3308 (Figure S5B). Global effects of HDAC3 inhibition on H3K27ac protein signal are similar in non-responder and responder cPDX models as expected (Figure S5B).

To further explore the effect of HDAC3 inhibition and ENZA treatment *in vitro*, we performed cell proliferation analyses using non-responder LuCaP 189.4 cPDX cells (Figure 5A). Vorinostat (pan-HDAC inhibitor) inhibits cell proliferation over time, both alone and in combination with ENZA (Figure 5B). Interestingly, there was no additional decrease of tumor cell proliferation when targeting HDAC3 specifically (BRD3308 and RGFP966), indicating that HDAC3-specific inhibition is on par with pan-HDAC inhibition with vorinostat (Figure S5D). For BRD3308, vorinostat performs better with respect to cell proliferation decrease (Figure S5D). For this reason and because vorinostat is clinically approved, we focused our analyses on vorinostat. Next, we performed *in vivo* intervention studies with cPDX LuCaP 189.4 cells. We studied tumor outgrowth in 4 treatment arms: (1) vehicle control (n = 10), (2) ENZA (n = 10), (3) vorinostat (n = 10), and (4) ENZA + vorinostat combination (n = 9). Vorinostat decreased tumor outgrowth both as a single agent (p = 0.0104) and combined with ENZA (p = 0.0709), while no response to ENZA as a single agent was observed, relative to control (Figure 5C; Table S3).

Given these findings, we hypothesized that HDAC3 works as a transcriptional regulator, potentially with GR as a partner, which is associated with the non-responder regions (Figure 4A) and is known to drive ENZA resistance in cell line and mouse models.[48] Previously, our lab reported HDAC3 as a GR interactor,[49] and others established that GR-mediated activation of target genes is facilitated by class I HDAC activity.[50] In our experiments, the GR agonist dexamethasone (Dexa) alone has no effect on H3K27ac signal in our non-responder regions in the non-responder model cPDX 189.4, while addition of vorinostat along with Dexa increases H3K27ac signal, and vorinostat alone shows the highest signal (Figure 5D). GR ChIP-seq analyses in our model confirmed that activated GR binds at non-responder H3K27ac sites (Figure 5E). Importantly, GR binding decreases when adding vorinostat (Figure 5E). We do not observe this change in GR binding upon vorinostat at gene TSSs in non-responder regions (within 50 kb of a non-responder peak), suggesting enhancer-centric epigenetic suppression of GR chromatin binding. With this, we propose a role for HDAC3 acting in combination with GR at ENZA resistance-associated enhancer regions, which is abrogated by the HDAC inhibitor vorinostat, blocking proliferation of ENZA-resistant prostate cancer cells.

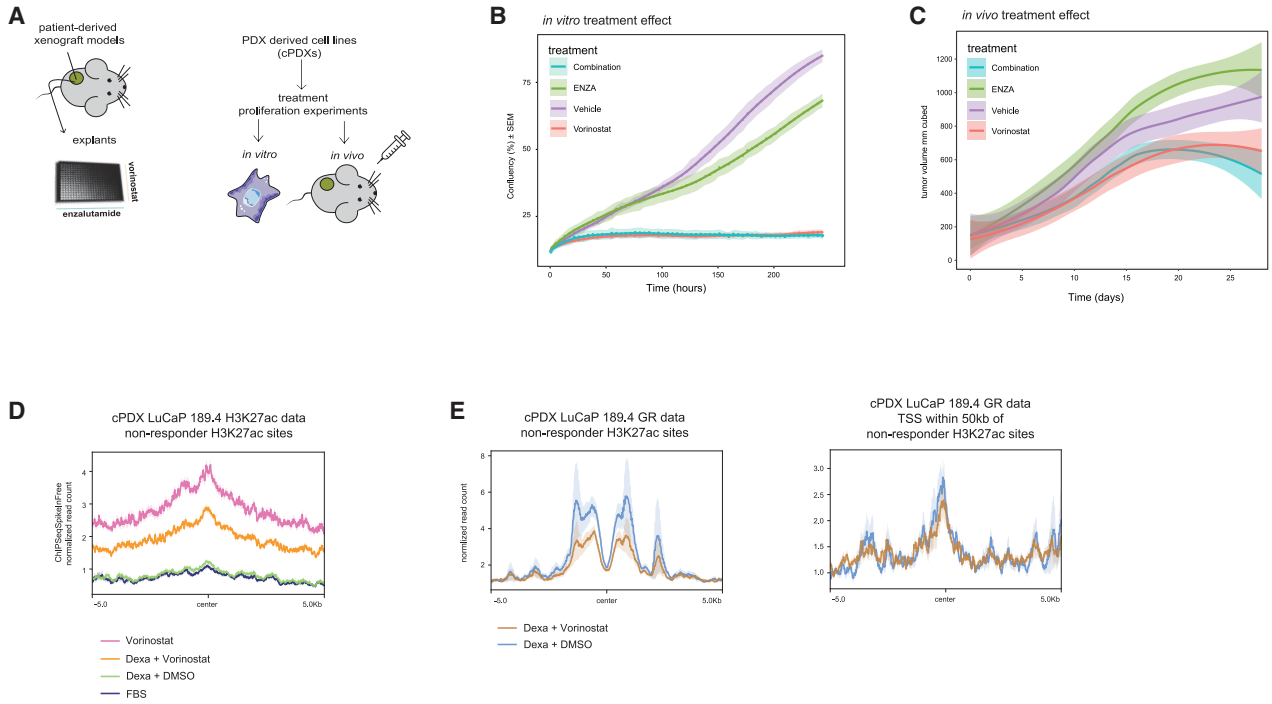

Figure 5. Treatment effect and mechanistic insight in non-responder cPDX

(A) Setup of analysis performed on patient-derived xenograft material, explants, (left) and *in vitro* and *in vivo* experiments (right) performed on cell lines derived from PDX (cPDX).

(B) Incucyte cell proliferation analyses, in response to treatment in non-responder model cPDX LuCaP 189.4 (*x* axis is time in hours, *y* axis is percent confluence [shading: ± standard error of the mean]). Lines represent cell confluence in vehicle (purple), vorinostat (pink), ENZA (green), and combination of vorinostat and ENZA (turquoise), each treatment type: biological triplicates with 6 technical replicates.

(C) *In vivo* mouse intervention experiments, showing smoothed tumor volume over time in mice injected with non-responder cPDX LuCaP 189.4 model cells (*x* axis time in treatment days, *y* axis tumor volume in cubic mm [shading: standard error of smoothed data]). After tumor outgrowth to 100 mm^3, mice were treated daily with vehicle (purple, $n = 10$), vorinostat (pink, $n = 10$), ENZA (green, $n = 10$), and combination of vorinostat and ENZA (turquoise, $n = 9$), biological replicates).

(D) Average ChIPseqSpikeInFree normalized H3K27ac read count profiles of merged data from cPDX LuCaP 189.4, at the 657 non-responder-enriched H3K27ac sites (±5 kb from the peak center) comparing FBS (dark blue), dexamethasone + DMSO (light green), dexamethasone + vorinostat (orange), and vorinostat alone (pink) ($n = 3$ biological replicates each). Shading indicates standard error of the data.

(E) (Left) Average normalized GR read count profiles of merged data from cPDX LuCaP 189.4, at the 657 non-responder-enriched H3K27ac sites (±5 kb from the peak center) comparing dexamethasone (Dexa) + DMSO (light blue) and Dexa + vorinostat (gold) ($n = 3$ replicates each). (Right) Average GR read count profiles of merged data from cPDX LuCaP 189.4, TSS sites found within 50 kb of a 657 non-responder-enriched H3K27ac site (±5 kb from the peak center) comparing Dexa + DMSO (light blue) and Dexa + vorinostat (gold) ($n = 3$ biological replicates each). Shading indicates standard error of the data.

See also Figure S5; Table S3.

DISCUSSION

The clinical significance of the non-protein coding genome in prostate cancer is rapidly gaining attention. Whole-genome sequencing of primary prostate cancer specimens revealed enrichment of somatic mutations in AR chromatin-binding sites,[51,52] a subset of which functionally affected enhancer activity.[17] Also in mCRPC, non-coding somatic alterations have been reported, including amplification of enhancer elements that regulate the expression of AR,[53,54] HOXB13,[18] and FOXA1.[18] Furthermore, extensive epigenetic reprogramming and AR enhancer plasticity have been related to tumorigenesis[8,17] and progression,[18] as well as therapy resistance.[19] To date, deviations in enhancer regulation have not been extensively studied in castration-resistant disease and remain unexplored in the context of a controlled clinical trial. Here, we interrogated the epigenome in relation to AR-targeted therapy response in patients with mCRPC. Within our clinical cohort, epigenetic features revealed a robust classification scheme predicting response to treatment, exposed potential drivers of resistance, and identified therapeutic drug combinations to combat castration-resistant disease.

While ENZA improves outcome in patients with mCRPC,[14,15] a significant proportion of patients with mCRPC experience no response to AR-targeting treatment due to intrinsic resistance mechanisms. Supporting this notion of pre-existing treatment resistance, H3K27ac profiles in mCRPC tumors remained unaltered following ENZA treatment, harboring epigenetic programs that support resistance-associated cellular growth. In contrast, most previously described resistance mechanisms appeared to be treatment-induced, including AR mutations[7,55,56] and amplification,[39] GR upregulation,[33–35] or enrichment of HNF4G.[32] As our patients already relapsed after prior therapies and developed castration resistance, the aforementioned

resistance mechanisms may have already occurred before our samples were taken. At the single-cell level, genes associated with our H3K27ac non-responder sites were significantly enriched in an ENZA resistance-associated cluster, which expands after long-term treatment,[28] indicating treatment-induced clonal selection. These results suggest divergent castration resistance mechanisms, which either sustain androgen dependency (as in the case for our "responder" population) or diverge toward complete resistance to AR-targeted drugs (our "non-responder" population), in which other transcription factors compensate.

Most transcription factors are generally considered challenging drug targets and other therapeutic strategies are urgently needed. Along these lines, for three of our hits: NKX3-1, FOXA1, and GATA2, specific inhibitors are yet to be developed. Recently, indirect small-molecule inhibition of FOXA1 has been described, by targeting EZH2[57] and LSD1,[58] presenting a potential direct therapeutic avenue in this setting.

As HDAC3 expression was reported critical for AR-driven transcriptional programs—both in hormone-sensitive and castration-resistant cell line models[59]—we chose to further explore HDAC inhibition as a therapeutic strategy. Our data reveal that HDAC3 is also critically involved in resistance to AR-targeted therapeutics in the mCRPC setting and demonstrate the efficacy of the pan-HDAC inhibitor vorinostat both alone and in conjunction with ENZA in cell line models, *ex vivo* in mCRPC PDX cultures, and *in vitro* and *in vivo* using cell lines derived from PDX models (cPDX LuCaP 189.4). This drug has been clinically approved for cutaneous T cell lymphomas and has also shown promise as a therapeutic strategy in advanced non-small cell lung cancer.[60] Although vorinostat showed no single-agent activity in patients with mCRPC, a phase 2 trial investigating the combination of the non-selective HDAC inhibitor panobinostat and the AR-targeted drug bicalutamide in 55 patients showed promising results.[61,62] Another trial[63] found no additional benefit of HDAC inhibition plus ENZA, which was in agreement with our *in vivo* experiment, where vorinostat alone sufficed to decrease tumor volume. To date, however, clinical trials in prostate cancer examining HDAC inhibition included very small numbers of patients, complicating interpretation thereof. Common drug-related serious adverse events such as thromboembolic events associated with vorinostat are of concern.[44] In line with this, in our *in vivo* experiments, mice treated with vorinostat or the combination of ENZA + vorinostat more often had diarrhea, which resulted in humane sacrifice. Our results support clinical efficacy evaluation of the combination of ENZA and vorinostat. Since vorinostat is aimed to modulate the development of ENZA resistance, treatment at a lower dose may reduce toxicity.

We identified HDAC1 and HDAC2 as well as enriched factors associated with non-responder H3K27ac sites (Figure 4A; Table S3, enrichment scores, 3.2 and 59.7, respectively). HDAC3 has previously been reported in cell lines to effectively drive resistance to AR-targeted therapies.[41,45,46] Consequently, we position HDAC3 as an exemplar of a biological process, and further follow-up studies would be required to disentangle the putative contributions of other HDAC family members. As GR—a known driver of ENZA resistance[48]—was prominent in our enrichment analysis (Figure 4A), we hypothesized that HDAC3 was working as a transcriptional regulator with GR to affect cell proliferation. Supporting this, we identified GR chromatin binding to be markedly reduced at H3K27ac resistance-associated sites following vorinostat treatment, indicating that GR-chromatin interactions may be responsible for the therapeutic effect we observe. Further follow-up studies would be required to pinpoint the specific regulatory regions driving the treatment-resistant phenotype.

While other studies have confirmed epigenetic profiles associated with response in the primary setting,[16] we now provide—in context of a prospective clinical trial including metastatic patients—an epigenetics-based biomarker for ENZA response in mCRPC. By analyzing these regions, we discovered the target HDAC3 and confirmed its importance in treatment intervention experiments using the pan-HDAC inhibitor vorinostat, which significantly lowered tumor growth *in vivo*. We have also elucidated potential mechanistic insights pointing to GR action at our resistance-associated sites, a driver of ENZA resistance previously reported in preclinical studies, in which we now provide further clinical support. Recently developed cell-free ChIP-seq methodologies on patient plasma allow for the epigenetic interrogation of prostate cancer metastases in a minimally invasive manner.[64] Future developments on these approaches may allow for the implementation of our epigenetic signature in clinical routine, to identify those patients upfront with a likely poor response to ENZA alone and consider these patients eligible for combination treatment strategies. Based on our results, new clinical trials for testing vorinostat—or other HDAC inhibitors—potentially in conjunction with ENZA for patients with mCRPC would be justified, since drugs with effective therapeutic windows are urgently needed to combat this currently incurable stage of the disease.

Limitations of the study

We conducted a single-arm, open-label, phase 2 study in which 64 patients with progressive mCRPC scheduled to be treated with ENZA were included. The number and nature of pre-treatments were not defined in the inclusion and exclusion criteria. Consequently, the pre-treatments of the patients varied, possibly affecting clinical outcomes and outcomes of the translational studies. Furthermore, patients were included between 2014 and 2019. Consequently, a proportion of patients in the trial were not treated as extensive in the metastatic castration-sensitive stage of the disease and were not treated with radium-223 and/or 177Lu-prostate-specific membrane antigen (PSMA) prior to docetaxel in the mCRPC stage of the disease, as present patients would be treated. Furthermore, of the 64 patients in the study, a subset of 38 samples could be evaluated for translational studies, which might have introduced bias.

RESOURCE AVAILABILITY

Lead contact

Further information and requests for resources should be directed to the lead contact, Andries M. Bergman (a.bergman@nki.nl).

Materials availability

This study did not generate new, unique reagents.

Data and code availability

- The sequencing data reported in this paper have been deposited in the European Genome-Phenome Archive (EGA). EGA numbers: patient ChIP-seq data (EGAS00001006161) and LuCaP cell line ChIP-/RNA-seq data (EGAD50000001345 and EGAD50000001344, respectively).
- This study did not report new original code.
- Any additional information required to reanalyze the data reported in this work paper is available from the lead contact upon request.

ACKNOWLEDGMENTS

The authors gratefully acknowledge the patients and the families of patients who contributed to this study. We thank the Netherlands Cancer Institute (NKI) Genomics Core Facility, Core Facility Molecular Pathology and Biobanking, Research High Performance Computing Facility, Scientific Information Service, and our colleagues of the NKI Preclinical Intervention Unit of the Mouse Clinic for Cancer and Aging (MCCA) for technical support in animal experiments. We also thank all group members from the Zwart, Bergman, and Corey labs for highly constructive feedback and suggestions. The authors thank Kim van der Zande at the NKI for excellent clinical data support. Research at the NKI is supported by institutional grants of the Dutch Cancer Society and the Dutch Ministry of Health, Welfare and Sport. This work is part of the Oncode Institute, which is partly financed by the Dutch Cancer Society. This work was supported by Astellas Pharma Europe BV (W.Z. and A.M.B.); the Prostate Cancer Foundation (Challenge Award – M.L.F., M.P., W.Z., and T.M.S.); the United States Department of Defense (Idea Award, PC180367 – M.L.F., M.P., and W.Z.); Oncode Institute (W.Z.); KWF Dutch Cancer Society/Alpe d'HuZes (10084 – W.Z. and A.M.B.; 7080 – A.M.B., M.S.v.d.H., and L.W.); PNW Prostate Cancer SPORE (P50CA097186 and P01CA163227 – E.C. and P.S.N.); R01 CA234715, R01 CA266452, R21 CA277368-01, and PC230420 (P.S.N.); and Craig Watjen Memorial funds (E.C.). A.U. is supported by Norwegian Cancer Society grants 273672 and 198016, Research Council of Finland grant no. 349314, and Tampere Institute for Advanced Study. S.H. and M.N. are supported by the Research Council of Finland grant nos. 349314 and 310829.

AUTHOR CONTRIBUTIONS

T.M.S., E.M., Y.Z., S.P., W.Z., and A.M.B. wrote the main manuscript text. T.M.S., E.M., Y.Z., K.S., H.M.N., L.G.B., S.H., R.M., S.G., Y.K., J.K., S.L., S.S., C.L., M.S.v.d.H., M.N., V.v.d.N., J.S., B.M., G.J., G.J.L.H.v.L., R.L.B., A.U., P.S.N., E.C., S.P., W.Z., and A.M.B. prepared and analyzed data for all figures and tables. M.P., M.L.F., P.S.N., and L.W. reviewed the manuscript. All authors read, edited, and approved the manuscript.

DECLARATION OF INTERESTS

W.Z. and A.M.B. received research funding from Astellas Pharma for the work performed in this manuscript. P.S.N. has served as a paid consultant to AstraZeneca, Janssen, Pfizer, and Genentech and received research support from Janssen for work unrelated to the present study.

STAR★METHODS

Detailed methods are provided in the online version of this paper and include the following:

- KEY RESOURCES TABLE
- EXPERIMENTAL MODEL AND STUDY PARTICIPANT DETAILS
  - Clinical study design and participants
  - Patient derived xenograft (PDX) models
  - Cell line models and culture conditions
  - *In vivo* PDX derived cell line tumor models
- METHOD DETAILS
  - ChIP-seq sample processing and library preparation
  - ChIP-seq data analysis
  - RNA sample processing and sequencing
  - siRNA proliferation assay and screen analysis
  - Response to castration in PDX models
  - Drug synergy assessment in cell lines and explants
  - PDX derived cell line proliferation assays
  - Western blotting
  - *In vivo* PDX derived cell line injection and monitoring of tumor growth
- QUANTIFICATION AND STATISTICAL ANALYSIS
- ADDITIONAL RESOURCES

SUPPLEMENTAL INFORMATION

Supplemental information can be found online at https://doi.org/10.1016/j.xcrm.2025.102215.

Received: February 24, 2023
Revised: February 20, 2025
Accepted: June 5, 2025
Published: July 2, 2025

REFERENCES

1. Bray, F., Laversanne, M., Sung, H., Ferlay, J., Siegel, R.L., Soerjomataram, I., and Jemal, A. (2024). Global cancer statistics 2022: GLOBOCAN estimates of incidence and mortality worldwide for 36 cancers in 185 countries. CA Cancer J. Clin. *74*, 229–263. https://doi.org/10.3322/caac.21834.
2. Mottet, N., van den Bergh, R.C.N., Briers, E., Van den Broeck, T., Cumberbatch, M.G., De Santis, M., Fanti, S., Fossati, N., Gandaglia, G., Gillessen, S., et al. (2021). EAU-EANM-ESTRO-ESUR-SIOG Guidelines on Prostate Cancer-2020 Update. Part 1: Screening, Diagnosis, and Local Treatment with Curative Intent. Eur. Urol. *79*, 243–262. https://doi.org/10.1016/j.eururo.2020.09.042.
3. Freedland, S.J., Humphreys, E.B., Mangold, L.A., Eisenberger, M., Dorey, F.J., Walsh, P.C., and Partin, A.W. (2005). Risk of prostate cancer-specific mortality following biochemical recurrence after radical prostatectomy. JAMA *294*, 433–439. https://doi.org/10.1001/jama.294.4.433.
4. Kupelian, P.A., Mahadevan, A., Reddy, C.A., Reuther, A.M., and Klein, E.A. (2006). Use of different definitions of biochemical failure after external beam radiotherapy changes conclusions about relative treatment efficacy for localized prostate cancer. Urology *68*, 593–598. https://doi.org/10.1016/j.urology.2006.03.075.
5. Roehl, K.A., Han, M., Ramos, C.G., Antenor, J.A.V., and Catalona, W.J. (2004). Cancer progression and survival rates following anatomical radical retropubic prostatectomy in 3,478 consecutive patients: long-term results. J. Urol. *172*, 910–914. https://doi.org/10.1097/01.ju.0000134888.22332.bb.
6. Harris, W.P., Mostaghel, E.A., Nelson, P.S., and Montgomery, B. (2009). Androgen deprivation therapy: progress in understanding mechanisms of resistance and optimizing androgen depletion. Nat. Clin. Pract. Urol. *6*, 76–85. https://doi.org/10.1038/ncpuro1296.
7. Prekovic, S., van Royen, M.E., Voet, A.R.D., Geverts, B., Houtman, R., Melchers, D., Zhang, K.Y.J., Van den Broeck, T., Smeets, E., Spans, L., et al. (2016). The Effect of F877L and T878A Mutations on Androgen Receptor Response to Enzalutamide. Mol. Cancer Ther. *15*, 1702–1712. https://doi.org/10.1158/1535-7163.MCT-15-0892.
8. Pomerantz, M.M., Li, F., Takeda, D.Y., Lenci, R., Chonkar, A., Chabot, M., Cejas, P., Vazquez, F., Cook, J., Shivdasani, R.A., et al. (2015). The androgen receptor cistrome is extensively reprogrammed in human prostate tumorigenesis. Nat. Genet. *47*, 1346–1351. https://doi.org/10.1038/ng.3419.
9. Stelloo, S., Nevedomskaya, E., Kim, Y., Schuurman, K., Valle-Encinas, E., Lobo, J., Krijgsman, O., Peeper, D.S., Chang, S.L., Feng, F.Y.C., et al. (2018). Integrative epigenetic taxonomy of primary prostate cancer. Nat. Commun. *9*, 4900. https://doi.org/10.1038/s41467-018-07270-2.

10. Lupien, M., Eeckhoute, J., Meyer, C.A., Wang, Q., Zhang, Y., Li, W., Carroll, J.S., Liu, X.S., and Brown, M. (2008). FoxA1 translates epigenetic signatures into enhancer-driven lineage-specific transcription. Cell *132*, 958–970. https://doi.org/10.1016/j.cell.2008.01.018.

11. Wang, Q., Li, W., Zhang, Y., Yuan, X., Xu, K., Yu, J., Chen, Z., Beroukhim, R., Wang, H., Lupien, M., et al. (2009). Androgen receptor regulates a distinct transcription program in androgen-independent prostate cancer. Cell *138*, 245–256. https://doi.org/10.1016/j.cell.2009.04.056.

12. Kim, T.K., and Shiekhattar, R. (2015). Architectural and Functional Commonalities between Enhancers and Promoters. Cell *162*, 948–959. https://doi.org/10.1016/j.cell.2015.08.008.

13. Shlyueva, D., Stampfel, G., and Stark, A. (2014). Transcriptional enhancers: from properties to genome-wide predictions. Nat. Rev. Genet. *15*, 272–286. https://doi.org/10.1038/nrg3682.

14. Beer, T.M., Armstrong, A.J., Rathkopf, D.E., Loriot, Y., Sternberg, C.N., Higano, C.S., Iversen, P., Bhattacharya, S., Carles, J., Chowdhury, S., et al. (2014). Enzalutamide in metastatic prostate cancer before chemotherapy. N. Engl. J. Med. *371*, 424–433. https://doi.org/10.1056/NEJMoa1405095.

15. Scher, H.I., Fizazi, K., Saad, F., Taplin, M.E., Sternberg, C.N., Miller, K., de Wit, R., Mulders, P., Chi, K.N., Shore, N.D., et al. (2012). Increased survival with enzalutamide in prostate cancer after chemotherapy. N. Engl. J. Med. *367*, 1187–1197. https://doi.org/10.1056/NEJMoa1207506.

16. Linder, S., van der Poel, H.G., Bergman, A.M., Zwart, W., and Prekovic, S. (2018). Enzalutamide therapy for advanced prostate cancer: efficacy, resistance and beyond. Endocr. Relat. Cancer *26*, R31–R52. https://doi.org/10.1530/ERC-18-0289.

17. Mazrooei, P., Kron, K.J., Zhu, Y., Zhou, S., Grillo, G., Mehdi, T., Ahmed, M., Severson, T.M., Guilhamon, P., Armstrong, N.S., et al. (2019). Cistrome Partitioning Reveals Convergence of Somatic Mutations and Risk Variants on Master Transcription Regulators in Primary Prostate Tumors. Cancer Cell *36*, 674–689.e6. https://doi.org/10.1016/j.ccell.2019.10.005.

18. Pomerantz, M.M., Qiu, X., Zhu, Y., Takeda, D.Y., Pan, W., Baca, S.C., Gusev, A., Korthauer, K.D., Severson, T.M., Ha, G., et al. (2020). Prostate cancer reactivates developmental epigenomic programs during metastatic progression. Nat. Genet. *52*, 790–799. https://doi.org/10.1038/s41588-020-0664-8.

19. Stelloo, S., Nevedomskaya, E., van der Poel, H.G., de Jong, J., van Leenders, G.J.L.H., Jenster, G., Wessels, L.F.A., Bergman, A.M., and Zwart, W. (2015). Androgen receptor profiling predicts prostate cancer outcome. EMBO Mol. Med. *7*, 1450–1464. https://doi.org/10.15252/emmm.201505424.

20. Severson, T.M., Zhu, Y., De Marzo, A.M., Jones, T., Simons, J.W., Nelson, W.G., Yegnasubramanian, S., Freedman, M.L., Wessels, L., Bergman, A. M., et al. (2021). Epigenetic and transcriptional analysis reveals a core transcriptional program conserved in clonal prostate cancer metastases. Mol. Oncol. *15*, 1942–1955. https://doi.org/10.1002/1878-0261.12923.

21. Stelloo, S., Nevedomskaya, E., Kim, Y., Hoekman, L., Bleijerveld, O.B., Mirza, T., Wessels, L.F.A., van Weerden, W.M., Altelaar, A.F.M., Bergman, A.M., and Zwart, W. (2018). Endogenous androgen receptor proteomic profiling reveals genomic subcomplex involved in prostate tumorigenesis. Oncogene *37*, 313–322. https://doi.org/10.1038/onc.2017.330.

22. Ross-Innes, C.S., Stark, R., Teschendorff, A.E., Holmes, K.A., Ali, H.R., Dunning, M.J., Brown, G.D., Gojis, O., Ellis, I.O., Green, A.R., et al. (2012). Differential oestrogen receptor binding is associated with clinical outcome in breast cancer. Nature *481*, 389–393. https://doi.org/10.1038/nature10730.

23. Wang, Y., Song, C., Zhao, J., Zhang, Y., Zhao, X., Feng, C., Zhang, G., Zhu, J., Wang, F., Qian, F., et al. (2023). SEdb 2.0: a comprehensive super-enhancer database of human and mouse. Nucleic Acids Res. *51*, D280–D290. https://doi.org/10.1093/nar/gkac968.

24. He, Y., Wei, T., Ye, Z., Orme, J.J., Lin, D., Sheng, H., Fazli, L., Jeffrey Karnes, R., Jimenez, R., Wang, L., et al. (2021). A noncanonical AR addiction drives enzalutamide resistance in prostate cancer. Nat. Commun. *12*, 1521. https://doi.org/10.1038/s41467-021-21860-7.

25. Prensner, J.R., Chen, W., Han, S., Iyer, M.K., Cao, Q., Kothari, V., Evans, J. R., Knudsen, K.E., Paulsen, M.T., Ljungman, M., et al. (2014). The long non-coding RNA PCAT-1 promotes prostate cancer cell proliferation through cMyc. Neoplasia *16*, 900–908. https://doi.org/10.1016/j.neo.2014.09.001.

26. Yamamoto, H., Oue, N., Sato, A., Hasegawa, Y., Yamamoto, H., Matsubara, A., Yasui, W., and Kikuchi, A. (2010). Wnt5a signaling is involved in the aggressiveness of prostate cancer and expression of metalloproteinase. Oncogene *29*, 2036–2046. https://doi.org/10.1038/onc.2009.496.

27. Nguyen, H.M., Vessella, R.L., Morrissey, C., Brown, L.G., Coleman, I.M., Higano, C.S., Mostaghel, E.A., Zhang, X., True, L.D., Lam, H.M., et al. (2017). LuCaP Prostate Cancer Patient-Derived Xenografts Reflect the Molecular Heterogeneity of Advanced Disease an–d Serve as Models for Evaluating Cancer Therapeutics. Prostate *77*, 654–671. https://doi.org/10.1002/pros.23313.

28. Taavitsainen, S., Engedal, N., Cao, S., Handle, F., Erickson, A., Prekovic, S., Wetterskog, D., Tolonen, T., Vuorinen, E.M., Kiviaho, A., et al. (2021). Single-cell ATAC and RNA sequencing reveal pre-existing and persistent cells associated with prostate cancer relapse. Nat. Commun. *12*, 5307. https://doi.org/10.1038/s41467-021-25624-1.

29. Layer, R.M., Pedersen, B.S., DiSera, T., Marth, G.T., Gertz, J., and Quinlan, A.R. (2018). GIGGLE: a search engine for large-scale integrated genome analysis. Nat. Methods *15*, 123–126. https://doi.org/10.1038/nmeth.4556.

30. Mei, S., Qin, Q., Wu, Q., Sun, H., Zheng, R., Zang, C., Zhu, M., Wu, J., Shi, X., Taing, L., et al. (2017). Cistrome Data Browser: a data portal for ChIP-Seq and chromatin accessibility data in human and mouse. Nucleic Acids Res. *45*, D658–D662. https://doi.org/10.1093/nar/gkw983.

31. Zheng, R., Wan, C., Mei, S., Qin, Q., Wu, Q., Sun, H., Chen, C.H., Brown, M., Zhang, X., Meyer, C.A., and Liu, X.S. (2019). Cistrome Data Browser: expanded datasets and new tools for gene regulatory analysis. Nucleic Acids Res. *47*, D729–D735. https://doi.org/10.1093/nar/gky1094.

32. Shukla, S., Cyrta, J., Murphy, D.A., Walczak, E.G., Ran, L., Agrawal, P., Xie, Y., Chen, Y., Wang, S., Zhan, Y., et al. (2017). Aberrant Activation of a Gastrointestinal Transcriptional Circuit in Prostate Cancer Mediates Castration Resistance. Cancer Cell *32*, 792–806.e7. https://doi.org/10.1016/j.ccell.2017.10.008.

33. Li, J., Alyamani, M., Zhang, A., Chang, K.H., Berk, M., Li, Z., Zhu, Z., Petro, M., Magi-Galluzzi, C., Taplin, M.E., et al. (2017). Aberrant corticosteroid metabolism in tumor cells enables GR takeover in enzalutamide resistant prostate cancer. eLife *6*, e20183. https://doi.org/10.7554/eLife.20183.

34. Puhr, M., Hoefer, J., Eigentler, A., Ploner, C., Handle, F., Schaefer, G., Kroon, J., Leo, A., Heidegger, I., Eder, I., et al. (2018). The Glucocorticoid Receptor Is a Key Player for Prostate Cancer Cell Survival and a Target for Improved Antiandrogen Therapy. Clin. Cancer Res. *24*, 927–938. https://doi.org/10.1158/1078-0432.CCR-17-0989.

35. Shah, N., Wang, P., Wongvipat, J., Karthaus, W.R., Abida, W., Armenia, J., Rockowitz, S., Drier, Y., Bernstein, B.E., Long, H.W., et al. (2017). Regulation of the glucocorticoid receptor via a BET-dependent enhancer drives antiandrogen resistance in prostate cancer. eLife *6*, e27861. https://doi.org/10.7554/eLife.27861.

36. Jones, D., Wade, M., Nakjang, S., Chaytor, L., Grey, J., Robson, C.N., and Gaughan, L. (2015). FOXA1 regulates androgen receptor variant activity in models of castrate-resistant prostate cancer. Oncotarget *6*, 29782–29794. https://doi.org/10.18632/oncotarget.4927.

37. Culig, Z., Hoffmann, J., Erdel, M., Eder, I.E., Hobisch, A., Hittmair, A., Bartsch, G., Utermann, G., Schneider, M.R., Parczyk, K., and Klocker, H. (1999). Switch from antagonist to agonist of the androgen receptor bicalutamide is associated with prostate tumour progression in a new model system. Br. J. Cancer *81*, 242–251. https://doi.org/10.1038/sj.bjc.6690684.

38. Bishop, J.L., Thaper, D., Vahid, S., Davies, A., Ketola, K., Kuruma, H., Jama, R., Nip, K.M., Angeles, A., Johnson, F., et al. (2017). The Master Neural Transcription Factor BRN2 Is an Androgen Receptor-Suppressed

Driver of Neuroendocrine Differentiation in Prostate Cancer. Cancer Discov. *7*, 54–71. https://doi.org/10.1158/2159-8290.CD-15-1263.

39. Kregel, S., Chen, J.L., Tom, W., Krishnan, V., Kach, J., Brechka, H., Fessenden, T.B., Isikbay, M., Paner, G.P., Szmulewitz, R.Z., and Vander Griend, D.J. (2016). Acquired resistance to the second-generation androgen receptor antagonist enzalutamide in castration-resistant prostate cancer. Oncotarget *7*, 26259–26274. https://doi.org/10.18632/oncotarget.8456.

40. Chaytor, L., Simcock, M., Nakjang, S., Heath, R., Walker, L., Robson, C., Jones, D., and Gaughan, L. (2019). The Pioneering Role of GATA2 in Androgen Receptor Variant Regulation Is Controlled by Bromodomain and Extraterminal Proteins in Castrate-Resistant Prostate Cancer. Mol. Cancer Res. *17*, 1264–1278. https://doi.org/10.1158/1541-7786.MCR-18-1231.

41. McLeod, A.B., Stice, J.P., Wardell, S.E., Alley, H.M., Chang, C.Y., and McDonnell, D.P. (2018). Validation of histone deacetylase 3 as a therapeutic target in castration-resistant prostate cancer. Prostate *78*, 266–277. https://doi.org/10.1002/pros.23467.

42. Malik, R., Khan, A.P., Asangani, I.A., Cieślik, M., Prensner, J.R., Wang, X., Iyer, M.K., Jiang, X., Borkin, D., Escara-Wilke, J., et al. (2015). Targeting the MLL complex in castration-resistant prostate cancer. Nat. Med. *21*, 344–352. https://doi.org/10.1038/nm.3830.

43. Liu, J., Yu, Y., Kelly, J., Sha, D., Alhassan, A.B., Yu, W., Maletic, M.M., Duffy, J.L., Klein, D.J., Holloway, M.K., et al. (2020). Discovery of Highly Selective and Potent HDAC3 Inhibitors Based on a 2-Substituted Benzamide Zinc Binding Group. ACS Med. Chem. Lett. *11*, 2476–2483. https://doi.org/10.1021/acsmedchemlett.0c00462.

44. Olsen, E.A., Kim, Y.H., Kuzel, T.M., Pacheco, T.R., Foss, F.M., Parker, S., Frankel, S.R., Chen, C., Ricker, J.L., Arduino, J.M., and Duvic, M. (2007). Phase IIb multicenter trial of vorinostat in patients with persistent, progressive, or treatment refractory cutaneous T-cell lymphoma. J. Clin. Oncol. *25*, 3109–3115. https://doi.org/10.1200/JCO.2006.10.2434.

45. Butler, L.M., Agus, D.B., Scher, H.I., Higgins, B., Rose, A., Cordon-Cardo, C., Thaler, H.T., Rifkind, R.A., Marks, P.A., and Richon, V.M. (2000). Suberoylanilide hydroxamic acid, an inhibitor of histone deacetylase, suppresses the growth of prostate cancer cells in vitro and in vivo. Cancer Res. *60*, 5165–5170.

46. Marrocco, D.L., Tilley, W.D., Bianco-Miotto, T., Evdokiou, A., Scher, H.I., Rifkind, R.A., Marks, P.A., Richon, V.M., and Butler, L.M. (2007). Suberoylanilide hydroxamic acid (vorinostat) represses androgen receptor expression and acts synergistically with an androgen receptor antagonist to inhibit prostate cancer cell proliferation. Mol. Cancer Ther. *6*, 51–60. https://doi.org/10.1158/1535-7163.MCT-06-0144.

47. Biersack, B., Nitzsche, B., and Höpfner, M. (2022). HDAC inhibitors with potential to overcome drug resistance in castration-resistant prostate cancer. Cancer Drug Resist. *5*, 64–79. https://doi.org/10.20517/cdr.2021.105.

48. Arora, V.K., Schenkein, E., Murali, R., Subudhi, S.K., Wongvipat, J., Balbas, M.D., Shah, N., Cai, L., Efstathiou, E., Logothetis, C., et al. (2013). Glucocorticoid receptor confers resistance to antiandrogens by bypassing androgen receptor blockade. Cell *155*, 1309–1322. https://doi.org/10.1016/j.cell.2013.11.012.

49. Prekovic, S., Schuurman, K., Mayayo-Peralta, I., Manjón, A.G., Buijs, M., Yavuz, S., Wellenstein, M.D., Barrera, A., Monkhorst, K., Huber, A., et al. (2021). Glucocorticoid receptor triggers a reversible drug-tolerant dormancy state with acquired therapeutic vulnerabilities in lung cancer. Nat. Commun. *12*, 4360. https://doi.org/10.1038/s41467-021-24537-3.

50. Kadiyala, V., Patrick, N.M., Mathieu, W., Jaime-Frias, R., Pookhao, N., An, L., and Smith, C.L. (2013). Class I lysine deacetylases facilitate glucocorticoid-induced transcription. J. Biol. Chem. *288*, 28900–28912. https://doi.org/10.1074/jbc.M113.505115.

51. Morova, T., McNeill, D.R., Lallous, N., Gönen, M., Dalal, K., Wilson, D.M., 3rd, Gürsoy, A., Keskin, Ö., and Lack, N.A. (2020). Androgen receptor-binding sites are highly mutated in prostate cancer. Nat. Commun. *11*, 832. https://doi.org/10.1038/s41467-020-14644-y.

52. Zhou, S., Hawley, J.R., Soares, F., Grillo, G., Teng, M., Madani Tonekaboni, S.A., Hua, J.T., Kron, K.J., Mazrooei, P., Ahmed, M., et al. (2020). Noncoding mutations target cis-regulatory elements of the FOXA1 plexus in prostate cancer. Nat. Commun. *11*, 441. https://doi.org/10.1038/s41467-020-14318-9.

53. Quigley, D.A., Dang, H.X., Zhao, S.G., Lloyd, P., Aggarwal, R., Alumkal, J.J., Foye, A., Kothari, V., Perry, M.D., Bailey, A.M., et al. (2018). Genomic Hallmarks and Structural Variation in Metastatic Prostate Cancer. Cell *174*, 758–769.e9. https://doi.org/10.1016/j.cell.2018.06.039.

54. Takeda, D.Y., Spisak, S., Seo, J.H., Bell, C., O'Connor, E., Korthauer, K., Ribli, D., Csabai, I., Solymosi, N., Szallasi, Z., et al. (2018). A Somatically Acquired Enhancer of the Androgen Receptor Is a Noncoding Driver in Advanced Prostate Cancer. Cell *174*, 422–432.e13. https://doi.org/10.1016/j.cell.2018.05.037.

55. Korpal, M., Korn, J.M., Gao, X., Rakiec, D.P., Ruddy, D.A., Doshi, S., Yuan, J., Kovats, S.G., Kim, S., Cooke, V.G., et al. (2013). An F876L mutation in androgen receptor confers genetic and phenotypic resistance to MDV3100 (enzalutamide). Cancer Discov. *3*, 1030–1043. https://doi.org/10.1158/2159-8290.CD-13-0142.

56. Sun, C., Shi, Y., Xu, L.L., Nageswararao, C., Davis, L.D., Segawa, T., Dobi, A., McLeod, D.G., and Srivastava, S. (2006). Androgen receptor mutation (T877A) promotes prostate cancer cell growth and cell survival. Oncogene *25*, 3905–3913. https://doi.org/10.1038/sj.onc.1209424.

57. Park, S.H., Fong, K.W., Kim, J., Wang, F., Lu, X., Lee, Y., Brea, L.T., Wadosky, K., Guo, C., Abdulkadir, S.A., et al. (2021). Posttranslational regulation of FOXA1 by Polycomb and BUB3/USP7 deubiquitin complex in prostate cancer. Sci. Adv. *7*, eabe2261. https://doi.org/10.1126/sciadv.abe2261.

58. Gao, S., Chen, S., Han, D., Wang, Z., Li, M., Han, W., Besschetnova, A., Liu, M., Zhou, F., Barrett, D., et al. (2020). Chromatin binding of FOXA1 is promoted by LSD1-mediated demethylation in prostate cancer. Nat. Genet. *52*, 1011–1017. https://doi.org/10.1038/s41588-020-0681-7.

59. Welsbie, D.S., Xu, J., Chen, Y., Borsu, L., Scher, H.I., Rosen, N., and Sawyers, C.L. (2009). Histone deacetylases are required for androgen receptor function in hormone-sensitive and castrate-resistant prostate cancer. Cancer Res. *69*, 958–966. https://doi.org/10.1158/0008-5472.CAN-08-2216.

60. Gray, J.E., Saltos, A., Tanvetyanon, T., Haura, E.B., Creelan, B., Antonia, S.J., Shafique, M., Zheng, H., Dai, W., Saller, J.J., et al. (2019). Phase I/Ib Study of Pembrolizumab Plus Vorinostat in Advanced/Metastatic Non-Small Cell Lung Cancer. Clin. Cancer Res. *25*, 6623–6632. https://doi.org/10.1158/1078-0432.CCR-19-1305.

61. Bradley, D., Rathkopf, D., Dunn, R., Stadler, W.M., Liu, G., Smith, D.C., Pili, R., Zwiebel, J., Scher, H., and Hussain, M. (2009). Vorinostat in advanced prostate cancer patients progressing on prior chemotherapy (National Cancer Institute Trial 6862): trial results and interleukin-6 analysis: a study by the Department of Defense Prostate Cancer Clinical Trial Consortium and University of Chicago Phase 2 Consortium. Cancer *115*, 5541–5549. https://doi.org/10.1002/cncr.24597.

62. Ferrari, A.C., Alumkal, J.J., Stein, M.N., Taplin, M.E., Babb, J., Barnett, E.S., Gomez-Pinillos, A., Liu, X., Moore, D., DiPaola, R., and Beer, T.M. (2019). Epigenetic Therapy with Panobinostat Combined with Bicalutamide Rechallenge in Castration-Resistant Prostate Cancer. Clin. Cancer Res. *25*, 52–63. https://doi.org/10.1158/1078-0432.CCR-18-1589.

63. Lin, J., Elkon, J., Ricart, B., Palmer, E., Zevallos-Delgado, C., Noonepalle, S., Burgess, B., Siegel, R., Ma, Y., and Villagra, A. (2021). Phase I Study of Entinostat in Combination with Enzalutamide for Treatment of Patients with Metastatic Castration-Resistant Prostate Cancer. Oncologist *26*, e2136–e2142. https://doi.org/10.1002/onco.13957.

64. Berchuck, J.E., Baca, S.C., McClure, H.M., Korthauer, K., Tsai, H.K., Nuzzo, P.V., Kelleher, K.M., He, M., Steinharter, J.A., Zacharia, S., et al. (2022). Detecting Neuroendocrine Prostate Cancer Through Tissue-Informed Cell-Free DNA Methylation Analysis. Clin. Cancer Res. *28*, 928–938. https://doi.org/10.1158/1078-0432.CCR-21-3762.

65. Handle, F., Prekovic, S., Helsen, C., Van den Broeck, T., Smeets, E., Moris, L., Eerlings, R., Kharraz, S.E., Urbanucci, A., Mills, I.G., et al. (2019). Drivers of AR indifferent anti-androgen resistance in prostate cancer cells. Sci. Rep. *9*, 13786. https://doi.org/10.1038/s41598-019-50220-1.

66. Kim, S., Thaper, D., Bidnur, S., Toren, P., Akamatsu, S., Bishop, J.L., Colins, C., Vahid, S., and Zoubeidi, A. (2019). PEG10 is associated with treatment-induced neuroendocrine prostate cancer. J. Mol. Endocrinol. *63*, 39–49. https://doi.org/10.1530/JME-18-0226.

67. Li, H., and Durbin, R. (2009). Fast and accurate short read alignment with Burrows-Wheeler transform. Bioinformatics *25*, 1754–1760. https://doi.org/10.1093/bioinformatics/btp324.

68. Li, H., Handsaker, B., Wysoker, A., Fennell, T., Ruan, J., Homer, N., Marth, G., Abecasis, G., and Durbin, R.; 1000 Genome Project Data Processing Subgroup (2009). The Sequence Alignment/Map format and SAMtools. Bioinformatics *25*, 2078–2079. https://doi.org/10.1093/bioinformatics/btp352.

69. Zhang, Y., Liu, T., Meyer, C.A., Eeckhoute, J., Johnson, D.S., Bernstein, B. E., Nusbaum, C., Myers, R.M., Brown, M., Li, W., and Liu, X.S. (2008). Model-based analysis of ChIP-Seq (MACS). Genome Biol. *9*, R137. https://doi.org/10.1186/gb-2008-9-9-r137.

70. Marinov, G.K., Kundaje, A., Park, P.J., and Wold, B.J. (2014). Large-scale quality analysis of published ChIP-seq data. G3 (Bethesda) *4*, 209–223. https://doi.org/10.1534/g3.113.008680.

71. Ramirez, F., Ryan, D.P., Gruning, B., Bhardwaj, V., Kilpert, F., Richter, A. S., Heyne, S., Dundar, F., and Manke, T. (2016). deepTools2: a next generation web server for deep-sequencing data analysis. Nucleic Acids Res. *44*, W160–W165. https://doi.org/10.1093/nar/gkw257.

72. Lopez-Delisle, L., Rabbani, L., Wolff, J., Bhardwaj, V., Backofen, R., Grüning, B., Ramírez, F., and Manke, T. (2021). pyGenomeTracks: reproducible plots for multivariate genomic datasets. Bioinformatics *37*, 422–423. https://doi.org/10.1093/bioinformatics/btaa692.

73. Carr, D., Lewin-Koh, N., Maechler, M., Sarkar, D., and Pebesma, E. (2024). R package: hexbin (Hexagonal Binning Routines.URL). https://cran.r-project.org/web/packages/hexbin/index.html.

74. Yu, G., Wang, L.G., and He, Q.Y. (2015). ChIPseeker: an R/Bioconductor package for ChIP peak annotation, comparison and visualization. Bioinformatics *31*, 2382–2383. https://doi.org/10.1093/bioinformatics/btv145.

75. Quinlan, A.R., and Hall, I.M. (2010). BEDTools: a flexible suite of utilities for comparing genomic features. Bioinformatics *26*, 841–842. https://doi.org/10.1093/bioinformatics/btq033.

76. Shen, L. (2025). R package: GeneOverlap: Test and visualize gene overlaps. https://doi.org/10.18129/B9.bioc.GeneOverlap.

77. Wickham, H. (2016). ggplot2: Elegant Graphics for Data Analysis (Springer-Verlag).

78. Hao, Y., Hao, S., Andersen-Nissen, E., Mauck, W.M., 3rd, Zheng, S., Butler, A., Lee, M.J., Wilk, A.J., Darby, C., Zager, M., et al. (2021). Integrated analysis of multimodal single-cell data. Cell *184*, 3573–3587.e29. https://doi.org/10.1016/j.cell.2021.04.048.

79. Kassambara, A. (2023). R package: ggpubr: 'ggplot2' Based Publication Ready Plots.URL: https://ggplot2.tidyverse.org.

80. McKenna, A., Hanna, M., Banks, E., Sivachenko, A., Cibulskis, K., Kernytsky, A., Garimella, K., Altshuler, D., Gabriel, S., Daly, M., and DePristo, M. A. (2010). The Genome Analysis Toolkit: a MapReduce framework for analyzing next-generation DNA sequencing data. Genome Res. *20*, 1297–1303. https://doi.org/10.1101/gr.107524.110.

81. Jin, H., Kasper, L.H., Larson, J.D., Wu, G., Baker, S.J., Zhang, J., and Fan, Y. (2020). ChIPseqSpikeInFree: a ChIP-seq normalization approach to reveal global changes in histone modifications without spike-in. Bioinformatics *36*, 1270–1272. https://doi.org/10.1093/bioinformatics/btz720.

82. Kim, D., Paggi, J.M., Park, C., Bennett, C., and Salzberg, S.L. (2019). Graph-based genome alignment and genotyping with HISAT2 and HISAT-genotype. Nat. Biotechnol. *37*, 907–915. https://doi.org/10.1038/s41587-019-0201-4.

83. Anders, S., Pyl, P.T., and Huber, W. (2015). HTSeq–a Python framework to work with high-throughput sequencing data. Bioinformatics *31*, 166–169. https://doi.org/10.1093/bioinformatics/btu638.

84. Ianevski, A., Giri, A.K., and Aittokallio, T. (2020). SynergyFinder 2.0: visual analytics of multi-drug combination synergies. Nucleic Acids Res. *48*, W488–W493. https://doi.org/10.1093/nar/gkaa216.

85. Scher, H.I., Morris, M.J., Stadler, W.M., Higano, C., Basch, E., Fizazi, K., Antonarakis, E.S., Beer, T.M., Carducci, M.A., Chi, K.N., et al. (2016). Trial Design and Objectives for Castration-Resistant Prostate Cancer: Updated Recommendations From the Prostate Cancer Clinical Trials Working Group 3. J. Clin. Oncol. *34*, 1402–1418. https://doi.org/10.1200/JCO.2015.64.2702.

86. Schwartz, L.H., Litière, S., de Vries, E., Ford, R., Gwyther, S., Mandrekar, S., Shankar, L., Bogaerts, J., Chen, A., Dancey, J., et al. (2016). RECIST 1.1-Update and clarification: From the RECIST committee. Eur. J. Cancer *62*, 132–137. https://doi.org/10.1016/j.ejca.2016.03.081.

87. Badrising, S.K., van der Noort, V., Hamberg, P., Coenen, J.L.L.M., Aarts, M.J., van Oort, I.M., van den Eertwegh, A.J.M., Los, M., van den Berg, H.P., Gelderblom, H., et al. (2016). Enzalutamide as a Fourth- or Fifth-Line Treatment Option for Metastatic Castration-Resistant Prostate Cancer. Oncology *91*, 267–273. https://doi.org/10.1159/000448219.

88. Khalaf, D.J., Annala, M., Taavitsainen, S., Finch, D.L., Oja, C., Vergidis, J., Zulfiqar, M., Sunderland, K., Azad, A.A., Kollmannsberger, C.K., et al. (2019). Optimal sequencing of enzalutamide and abiraterone acetate plus prednisone in metastatic castration-resistant prostate cancer: a multicentre, randomised, open-label, phase 2, crossover trial. Lancet Oncol. *20*, 1730–1739. https://doi.org/10.1016/S1470-2045(19)30688-6.

89. Severson, T.M., Kim, Y., Joosten, S.E.P., Schuurman, K., van der Groep, P., Moelans, C.B., Ter Hoeve, N.D., Manson, Q.F., Martens, J.W., van Deurzen, C.H.M., et al. (2018). Characterizing steroid hormone receptor chromatin binding landscapes in male and female breast cancer. Nat. Commun. *9*, 482. https://doi.org/10.1038/s41467-018-02856-2.

90. Singh, A.A., Schuurman, K., Nevedomskaya, E., Stelloo, S., Linder, S., Droog, M., Kim, Y., Sanders, J., van der Poel, H., Bergman, A.M., et al. (2019). Optimized ChIP-seq method facilitates transcription factor profiling in human tumors. Life Sci. Alliance *2*, e201800115. https://doi.org/10.26508/lsa.201800115.

91. Malo, N., Hanley, J.A., Cerquozzi, S., Pelletier, J., and Nadon, R. (2006). Statistical practice in high-throughput screening data analysis. Nat. Biotechnol. *24*, 167–175. https://doi.org/10.1038/nbt1186.

92. Pinheiro, J.C., and Bates, D.M. (2006). Mixed-Effects Models in S and S-PLUS (Springer). https://doi.org/10.1007/b98882.

STAR★METHODS

KEY RESOURCES TABLE

REAGENT or RESOURCE	SOURCE	IDENTIFIER
Antibodies		
Rabbit polyclonal anti-AR	Millipore	Cat#06-680; RRID:AB_310214
Goat polyclonal anti-FOXA1	Abcam	Cat#ab5089; RRID:AB_304744
Mouse monoclonal anti-FOXA1	Seven Hills Bioreagents	Cat#WMAB-2F83; RRID:AB_451717
Rabbit polyclonal anti-H3K27ac	Active motif	Cat#39133; RRID:AB_2561016
Rabbit polyclonal anti-HDAC3	Abcam	Cat#ab137704
Rabbit polyclonal anti-GR (D6H2L)	Cell Signaling Technology	Cat#12041S
Mouse polyclonal anti-HSP90 (F-8)	Santa Cruz	Cat#sc-13119; RRID: AB_675659
Mouse polyclonal anti-Actin	Millipore	Cat#MAB1501R
IRDye Donkey-α-Goat IgG Secondary antibody	LI-COR Biosciences	Cat#926-32213; RRID: AB_621848
IRDye Donkey-α-Mouse IgG Secondary antibody	LI-COR Biosciences	Cat#926-68072; RRID: AB_10953628
IRDye Donkey-α-Goat IgG Secondary antibody	LI-COR Biosciences	Cat#926-32214; RRID: AB_621846
Biological samples		
Biopsies from patients with metastatic castration resistant prostate cancer	This study	ClinicalTrials.gov: NCT01855477
Patient-derived prostate cancer xenografts	University of Washington	LuCaP
Chemicals, peptides, and recombinant proteins		
Dexamethasone	MedChemExpress	Cat#HY-14648
Vorinostat	MedChemExpress	Cat#HY-10221
Dimethyl sulfoxide (99.7% acroseal)	Thermo Fisher Scientific	Cat#326881000
Enzalutamide (powder, mice experiments)	MedChemExpress	Cat#HY-70002_1g
Enzalutamide (10mM in DMSO)	MedChemExpress	Cat#HY-70002
Methyltrienolone (R1881)	Sigma-aldrich	Cat#R0908
BRD3308	MedChemExpress	Cat#HY-19618
RGFP966	MedChemExpress	Cat#HY-13909
Disuccinimidyl glutarate (DSG)	COVACHEM	Cat#13301-1
Formaldehyde solution (37%)	Merck	Cat#1039991000
Protein A magnetic beads	Thermo Fisher Scientific	Cat#10008D
Protein G magnetic beads	Thermo Fisher Scientific	Cat#10009D
Lipofectamine RNAiMAX Reagent	Invitrogen	Cat#13778150
Cultrex RGF BME, type 2	Bio-Techne	Cat#3536-005-02
siGENOME Human FOXA1 siRNA (set of 4)	Dharmacon	Cat# MQ-010319-01-0002
siGENOME Human GATA2 siRNA (set of 4)	Dharmacon	Cat# MQ-009024-00-0002
siGENOME Human NKX3-1 siRNA (set of 4)	Dharmacon	Cat# MQ-015422-00-0002
siGENOME Human CREB1 siRNA (set of 4)	Dharmacon	Cat# MQ-003619-01-0002
siGENOME Human HDAC3 siRNA (set of 4)	Dharmacon	Cat# MQ-003496-02-0002
siGENOME Human TLE3 siRNA (set of 4)	Dharmacon	Cat# MQ-019929-01-0002
siGENOME Human PIAS1 siRNA (set of 4)	Dharmacon	Cat# MQ-008167-01-0002
siGENOME Human ASH2L siRNA (set of 4)	Dharmacon	Cat# MQ-019831-01-0002
siGENOME Human HOXB13 siRNA (set of 4)	Dharmacon	Cat# MQ-012226-01-0002
siGENOME Human NR3C1 siRNA (set of 4)	Dharmacon	Cat# MQ-003424-03-0002
siGENOME Human TOP1 siRNA (set of 4)	Dharmacon	Cat# MQ-005278-00-0002
siGENOME Human AR siRNA (set of 4)	Dharmacon	Cat# MQ-003400-02-0002
siGENOME Human HDAC2 siRNA (set of 4)	Dharmacon	Cat# MQ-003495-02-0002
siGENOME Human HNF4G siRNA (set of 4)	Dharmacon	Cat# MQ-003407-02-0002

(*Continued on next page*)

Continued

REAGENT or RESOURCE	SOURCE	IDENTIFIER
siGENOME Human SUMO2 siRNA (set of 4)	Dharmacon	Cat# MQ-016450-01-0002
Critical commercial assays		
RNeasy Mini Kit	Qiagen	Cat#74106
TruSeq Stranded mRNA sample preparation kit	Illumina Inc.	Cat#RS-122-2101/2
CellTiter-Glo Luminescent Cell Viability Assay	Promega	Cat#G7572
RNAGEM kit	MicroGEM	N/A
Quant-iT^{TM} RiboGreen^{TM} RNA Assay Kit	Thermo Fisher Scientific	Cat#R11490
SensiMix^{TM} SYBR Kit	Bioline	Cat#QT615-05
Miltenyi gentleMACS system with a Human Tumor dissociation kit	Miltenyi Corp.	Cat#130095929
Deposited data		
Patient ChIP-seq data	This study	EGA: EGAS00001006161
LuCaP cell line ChIP-seq data	This study	EGA: EGAD50000001345
LuCaP cell line RNA-seq data	This study	EGA: EGAD50000001344
PDX mCRPC H3K27ac ChIP-seq data	Pomerantz et al., 2020[18]	GEO: GSE130408
H3K27ac data from primary prostate cancer patient tumors	Stelloo et al., 2018[9]	GEO: GSE120738
SEdb 2.0 LNCaP data	Wang et al., 2023[23]	http://www.licpathway.net/sedb/
scRNA-seq from parental LNCaP cells	Handle et al., 2019 [65]	GEO: GSE130534
scRNA-seq from LNCaP RES-B	Taavitsainen et al., 2021[28]	GEO: GSE168669
Experimental models: Cell lines		
Human: LNCaP	ATCC	Cat# CRL-1740
Human: LNCaP-16D	Kim et al., 2029[66]	N/A
Human: LNCaP-abl	Culig et al., 1999[37]	N/A
Human: LNCaP-Enz^{R}	Kregel et al., 2016[39]	N/A
Human: PDX derived cell line LuCaP 35	Peter Nelson Laboratory	N/A
Human: PDX derived cell line LuCaP 189.4	Peter Nelson Laboratory	N/A
Experimental models: Organisms/strains		
Mouse: NOD-Scid IL2Rag null male mice	Jackson Laboratory	N/A
Mouse: intact C.B. 17 SCID male mice	Charles River	236
Oligonucleotides		
qPCR primer ACTB: F - 5′-CCTGGCACCCAGCACAAT-3′ R - 5′-GGGCCGGACTCGTCATACT-3′	This paper	N/A
qPCR primer FOXA1: F- 5′-GTGAAGATGGAAGGGCATGAA-3′ R - 5′-CCTGAGTTCATGTTGCTGACC-3′	This paper	N/A
qPCR primer ASH2L: F- 5′-CTGACGTCTTGTATCACGTG-3′ R - 5′-GCATCTTTGGGAGAACATTTG-3′	This paper	N/A
qPCR primer GATA2: F- 5′-GACAAGGACGGCGTCAAGTA-3′ R - 5′-GGTGCCCATAGTAGCTAGGC-3′	This paper	N/A
qPCR primer HDAC3: F- 5′-ACGGTGTCCTTCCACAAATACG-3′ R - 5′-GGTGCTTGTAACTCTGGTCATC-3′	This paper	N/A
Software and algorithms		
R v3.4.4/v4.0.3/v4.1.2	https://www.r-project.org/	https://www.r-project.org/
BWA (v0.5.20)	Li and Durbin., 2009[67]	https://bio-bwa.sourceforge.net/
Incucyte ZOOM 2018A	https://www.sartorius.com	https://www.sartorius.com

(*Continued on next page*)

Continued

REAGENT or RESOURCE	SOURCE	IDENTIFIER
samtools (v1.8)	Li et al., 2009[68]	https://www.htslib.org/
Picard Tools (v2.18)	Maintained by The Broad Institute	http://broadinstitute.github.io/picard/
Macs2 (v2.1.1)	Zhang et al., 2008[69]	https://pypi.org/project/MACS2/
Phantompeakqualtools	Marinov et al., 2014[70]	https://github.com/kundajelab/phantompeakqualtools
deepTools (v2.0)	Ramirez et al., 2016[71]	https://deeptools.readthedocs.io/en/latest/
pyGenomeTracks (v3.6)	Lopez-Delisle et al., 2021[72]	https://github.com/deeptools/pyGenomeTracks
DiffBind (v2.4.8)	Ross-Innes et al., 2012[22]	https://bioconductor.org/packages/release/bioc/html/DiffBind.html
hexbin (v1.28.1)	Carr D et al., 2025[73]	https://github.com/edzer/hexbin
ChIPSeeker (v1.26.2)	Yu et al., 2025[74]	https://bioconductor.org/packages/release/bioc/html/ChIPseeker.html
BEDTools (v2.26.0)	Quinlan et al., 2010[75]	https://bedtools.readthedocs.io/en/latest/
GeneOverlap (v1.30.0)	Shen, 2018[76]	http://bioconductor.jp/packages/3.8/bioc/vignettes/GeneOverlap/inst/doc/GeneOverlap.pdf
ggplot (v3.4.0)	Wickham, 2016[77]	https://ggplot2.tidyverse.org
Seurat (v4.3.0)	Hao et al., 2021[78]	https://satijalab.org/seurat/
ggpubr (v0.3.0)	Kassambara, 2023[79]	https://github.com/kassambara/ggpubr
CistromeDB Data Browser	Zheng et al., 2019[31]	http://cistrome.org/db/#/
GIGGLE search	Layer et al., 2018[29]	https://github.com/ryanlayer/giggle
ChIP-seq pipeline for hg38 analysis		https://github.com/sebastian-gregoricchio/SPACCa
gatk (v4.3.0.0)	McKenna et al. 2010[80]	https://github.com/broadinstitute/gatk/releases
ChIPseqSpikeInFree (v1.2.4)	Jin et al., 2020[81]	https://github.com/stjude/ChIPseqSpikeInFree
HISAT2 (v2.1.0)	Kim et al. 2019[82]	https://daehwankimlab.github.io/hisat2/
HTSeq count (v0.5.3)	Anders et al. 2014[83]	https://htseq.readthedocs.io/en/release_0.11.1/count.html
SynergyFinder 2.0	Ianevski et al., 2020[84]	https://synergyfinder.aittokallio.group/2025050914331658354/

EXPERIMENTAL MODEL AND STUDY PARTICIPANT DETAILS

Clinical study design and participants

We conducted a single-arm, open-label, phase 2 study, in patients with mCRPC at the Netherlands Cancer Institute. Male patients over 18 years of age, with histologically confirmed adenocarcinoma of the prostate, Eastern Cooperative Oncology Group (ECOG) performance status 0-2, a serum testosterone level <50 ng/dl, scheduled for ENZA treatment and not previously treated with ENZA, with progressive disease, defined as a PSA rise (PCWG3 criteria[85]) and/or radiographic progression (RECIST 1.1 criteria[86]) and metastatic lesions of which a histological biopsy could safely be obtained, were included in the trial. This single center cohort study was conducted as a sub-investigation of the CPCT-02 biopsy protocol (NCT01855477), which aims to analyze the individual metastatic cancer genome in patients, to develop future personal predictors for response to systemic treatment. This study was approved by the local medical ethics committee of the Netherlands Cancer Institute and was activated on January 24th, 2012. The protocol complied with the ethical principles of the Declaration of Helsinki. Patients provided signed informed consent for translational studies and recording and analysis of baseline characteristics and clinical outcomes of ENZA treatment. The trial was approved by the institutional review board of the Netherlands Cancer Institute, written informed consent was signed by all participants enrolled in the study, and all research was carried out in accordance with relevant guidelines and (inter-)national and ethical standards. Within the General Data Protection Regulation, patients always had the opportunity to object or actively consent to the (continued) use of their personal data and biospecimens for research purposes.

Clinical study trial procedure details

Baseline studies included radiographic evaluation (CT scan of thorax and abdomen), physical examination, ECOG performance score, blood cell counts and serum chemistry and a biopsy from a metastatic site. Subsequently, patients were treated with ENZA at a starting dose of 160 mg/day (4 tablets of 40 mg once daily). Dose adjustments to as low as 80 mg/day were allowed. During the course of ENZA treatment, physical examination, ECOG performance score, blood analysis, including PSA measurements, was

performed every four weeks at the outpatient clinic. A radiographic response was evaluated at 12 weeks by means of a CT scan of thorax and abdomen (RECIST1.1).[86] Patients with bone only metastases were considered progressive when new metastases were detected. In these patients, a response to treatment could not be evaluated. ENZA treatment was continued until progression or intolerance and selection of subsequent treatment. Frequency of visits to the outpatient clinic and assessments beyond ENZA treatment were at the discretion of the physician. Primary endpoint of the study is Time to PSA Progression (TTPP) defined as time from inclusion into the trial until date of a confirmed second PSA rise (PCWG3).[85] Secondary recorded clinical outcomes are, rate of $\geq$50% serum PSA decrease from baseline, radiographic response (RECIST 1.1 criteria)[86] and overall survival (OS) defined as time from inclusion into the trial until death.

For biomarker discovery purposes, we aimed to construct a cohort of ENZA treated patients at various lines of mCRPC treatment in a Phase 2 clinical trial, which is representative for the general population. The first line ENZA PREVAIL study[14] showed an 11.2 month (48.7 weeks) time to PSA progression (TTPP), while the second line ENZA AFFIRM study[15] showed an 8.3 month (36.1 weeks) TTPP. A retrospective study into ENZA treated patients in fourth or fifth line, suggested a TTPP of 3.6 months (15.7 weeks).[87] We assumed to enroll 20% of patients treated with ENZA as a first line treatment, 20% as a second and 60% of patients in a higher line of treatment. Consequently, we expect a TTPP in this miscellaneous population of 22 weeks. Inclusion of 60 patients will allow the detection of this median TTPP with 95% confidence intervals of 16.4-33.6 weeks. This expected range is sufficiently narrow, that when the true TTPP falls within these limits, it suggests that results of the trial are representative and can be interpreted clinically. All time-to-event endpoints were estimated by the Kaplan-Meier method. Differences in normally distributed baseline characteristics and study outcomes between the whole population and the evaluable pre-treatment biopsy and post-treatment biopsy sub populations were evaluated by a student t-test.

In Table S1, the baseline characteristics of all 64 included patients (whole population) are summarized. Median age of the patients was 69 years and the majority of patients had skeletal (75.0%) and/or lymph node (70.3%) metastases, while 34.4% had visceral organ metastases. Virtually all patients (93.8%) had PSA progression, while radiographic progression was established in 81.3% of patients prior to ENZA treatment. Approximately one-third of patients (32.8%) received ENZA as a first line mCRPC treatment, while all other patients previously received other treatments, including docetaxel chemotherapy (62.5%) and the AR-signaling targeting agent abiraterone (23.4%). Outcomes of treatment, after a median of 17 (IQR: 9-30) months follow-up, are summarized in Table S2. All patients in the trial were treated with ENZA (160 mg once daily), except for one patient who was treated with abiraterone instead. The median duration of treatment was 22.7 (IQR: 13-45) weeks and 46.9% of patients had a $\geq$ 50% decrease of serum PSA from baseline. Complete or partial radiological responses were found in 18.8% of patients and 17.2% of patients had radiologic stable disease after 12 weeks of treatment. The primary endpoint of the trial, Time to PSA progression (TTPP) was 17.7 (IQR 12-35) weeks, while median overall survival was 14.5 months.

Rate of PSA response in the current study (ENZA-treated in first, second and later treatment lines) was lower than in the randomized controlled trial of first line ENZA (PREVAIL trial),[14] but in line with the randomized controlled trial of second line ENZA (AFFIRM trial)[15] (54%). The primary endpoint of the trial, Time to PSA progression (TTPP) was 17.7 (IQR 12-35) weeks which falls within the expected range considering 23.4% of patients in the current trial were previously treated with abiraterone and consequently likely to have a lower likelihood of durable response due to cross-resistance.[88] However, the composition of patients in the trial, based on the line of treatment, deferred from the assumption that 60% percent of patients would have been treated with ENZA as a third or higher line of mCRPC treatment. This means that the trial population had fewer prior treatments than anticipated. The TTPP in the current trial was shorter than in the AFFIRM trial (36 weeks).[15] Complete or partial response was found in 18.8% of patients and 17.2% of patients had radiographic stable disease after 12 weeks of treatment. Overall survival was 14.5 months which was shorter than the 18.4 months, reported in the AFFIRM study.[15] In conclusion, ENZA treatment resulted in a TTPP within the expected range. The TTPP was shorter than in the registration studies PREVAIL and AFFIRM,[14,15] which is explained by the miscellaneous population with more pretreatments, most notably prior abiraterone.

Patient derived xenograft (PDX) models

All animal experiments were performed after University of Washington IACUC approval following ARRIVE and NIH guidelines. Subcutaneous tumors were implanted in intact C.B.17 SCID male mice (Charles River) and when tumors reached 100mm^3 animals were randomized to control and castrated groups. Tumor growth and body weights were monitored twice a week. Animals were sacrificed at the end of the study or when animals became compromised.

Cell line models and culture conditions

PDX derived cell line models

The cell lines derived from LUCaP 189.4 and 35 (cPDX LuCaP) were cultured in DMEM medium (Life Technologies) supplemented with 10% fetal bovine serum (FBS) and 1% Penicillin-Streptomycin in a 5% CO_2 atmosphere at 37°C. For GR-activation experiments with vorinostat, cells were cultured in DMEM supplemented with 10% FBS, 1% Penicillin-Streptomycin and 100 nM Dexamethasone (MedChemExpress) for 2 hours followed by another 2-hour treatment in presence of 5 μM vorinostat (MedChemExpress) or the DMSO (Fisher) vehicle control. For the experiments without dexamethasone stimulation the cells were only treated with 5 μM vorinostat (MedChemExpress) or DMSO vehicle control. For the AR-activation experiments, cells were hormone deprived for 3 days in

DMEM supplemented with 5% Dextran coated charcoal (DCC) stripped medium instead of FBS. Upon hormone deprivation, the cells were treated with 1 nM of the synthetic androgen R1881 (PerkinElmer) or DMSO (Fisher) for vehicle control.

Enzalutamide resistant cell line models

Castration-resistant prostate cancer models (LNCaP-Abl and LNCaP-16D[38]) were kindly provided by Helmut Klocker[37] and Amina Zoubeidi.[66] ENZA resistant LNCaP derivatives LNCaP-Enz^R were kindly provided by the Donald Vander Griend.[39] LNCaP-Abl cells were cultured in RPMI-1640 medium containing 10% DCC (hormone deprived FBS), LNCaP-16D[38] cells were cultured in RPMI-1640 medium supplemented with 10% FBS, and LNCaP-Enz^R cells were cultured in RPMI-1640 medium containing 10% FBS and 10μM ENZA. All cell lines were authenticated and tested for mycoplasma contamination.

In vivo PDX derived cell line tumor models

Intervention studies with NOD-Scid IL2Rgnull male mice (Jackson Laboratory USA) were carried out at the Netherlands Cancer Institute (NKI) according to local and international regulations and ethical guidelines, and were approved by the local and central animal experimental committee at the NKI (AVD30100202011584; EGP 24.1.11184). LuCaP 189.4 cells were subcutaneously implanted and tumors were measured and mice weighed 3 times per week. When the tumor became 100mm^3, mice were randomized to treatment group and treated for 28 days. When tumor became 1500mm^3 mice were sacrificed or when other humane endpoint was reached.

METHOD DETAILS

ChIP-seq sample processing and library preparation

Biopsy patient tissue samples were taken from a lymph-node metastasis or visceral metastasis selected by CT scan, while sites for a biopsy from a bone metastasis were selected by ^{68}Ga-PSMA PET scanning. Fresh-frozen metastatic biopsy samples from 64 CRPC patients were collected. The tumor percentage of these samples was scored on hematoxylin and eosin (H&E) stained slides by a dedicated pathologist. After tumor cell content was confirmed, the chromatin immunoprecipitations were performed as previously described.[20,89,90] In brief, lymph-node and visceral samples were cryo-sectioned into slices of 30μm, while bone samples were cryo-sectioned to slices of 10μm, and crosslinked using 2 mM disuccinimidyl glutarate (DSG, 20593; Thermo Fisher Scientific) for 25 min.

The cPDX LuCaP 189.4 and 35 cells were seeded with a cell density of 8×10^5 cells per 15 cm plate in FBS conditions. After seeding, the cells were treated with 100nM dexamethasone (MedChemExpress) for 2 hours followed by another 2-hour treatment of 5 μM vorinostat (MedChemExpress) or the respective vehicle condition according to the volume of their corresponding compound. For the experiments without dexamethasone stimulation the cells were only treated with 5 μM vorinostat (MedChemExpress) or its corresponding vehicle condition. After treatment, the LuCaP cell lines were fixed in 1% formaldehyde (Merck) for 10 minutes and quenched with 0.125M glycine. After collection of the cells and confirmation of the tumor cell percentage in the patient tissues, the samples were lysed and sonicated using the PicoBioruptor (Diagenode). For each sample, and each ChIP, 5μg of antibody and 50μl of either Protein A or Protein G magnetic beads (10008D or 10009D; Thermo Fisher Scientific) were used. Antibodies used were: AR (Millipore, 06-680), FOXA1 (Abcam, ab5089), H3K27ac (Active motif, 39133, HDAC3 (Abcam, ab137704) and GR (Cell Signaling Technology, 12041S).

Patient tissue sample sequencing libraries were prepared from the immunoprecipitated DNA using the KAPA library kit (KK8234, Roche) and sequenced using the Illumina HiSeq2500 (65 bp, single end). Each patient sample input DNA was used as matched control for sample ChIP-seq. Sequencing libraries from cPDX LuCaP 189.4 were prepared and sequenced using the Illumina NovaSeq 6000 (54bp, paired end). Input DNA for the LuCaP 189.4 cell line was used as control.

ChIP-seq data analysis

For patient samples, raw sequence data were aligned to hg19 using BWA[67] v0.5.20. Aligned reads were filtered for mapping quality (MQ) > 20 using samtools v1.8.[68] Duplicate reads were marked using Picard MarkDupes function v2.18 (http://broadinstitute.github.io/picard/). Peaks were called using macs2 (v2.1.1)[69] with the fragment size determined using Phantompeakqualtools[70] against corresponding input DNA for all samples. Phantompeakqualtools was used to identify the Relative Strand Cross-correlation (RSC)[70] and deepTools (v2.0)[71] to determine the fraction of reads in peaks (FRiP) and readcounts. Samples with RSC > 0.7, FRiP ≥ 1.0 and ≥ 8,000 peaks were kept for further analysis (Table S3). Snapshots of raw signal were generated using pyGenomeTracks (v3.6) with bigwig files.[72] Bigwig files were generated from aligned bam files using deepTools v2.0 bamCoverage function. To correlate read count data in 50kb bins across the genome for all samples and PDX samples, deepTools computeMatrix function was used on bigwigs followed by plotCorrelation. Visualization of raw reads was carried out with bigwigs using deepTools (v2.0) computeMatrix, plotHeatmap and plotProfile functions. For visualizing profiles of binding data between groups (non-responders/responders) at specific regions, aligned files from the samples within groups were merged and subsequently normalized by downsampling to equivalent read counts (~20 million reads) using samtools and visualized using deepTools plotProfile. Principal component analysis was carried out using plotPCA function with the reads counted in peaks (dba.count function) from DiffBind package v2.4.8 in R v3.4.4. Supervised differential analyses using dba.analyze and resulting heatmap and volcano plot were generated using the DiffBind package (v2.4.8 in R v3.4.4)[22] with the reads counted in peaks using the dba.count function using default DESeq2 method. Volcano plot hexbin density

tiles were plotted with R package hexbin (v1.28.1).[73] Genomic features and genes were assigned to differential peaksets using ChIPSeeker (v1.26.2)[74] in R (v4.0.3). Genes with a TSS within 50kb of a peak were considered associated genes.

To identify association of 657 non-responder H3K27ac sites with super-enhancers, the SEdb 2.0 LNCaP data were downloaded[23] and lifted over to hg19. This file and the 657 sites file were used as input in BEDTools fisher exact test (v2.26.0) incorporating the size of the human genome hg19[75] to determine if the number of overlaps between the two files is significantly more than expected by chance given the size of the human genome. To test for enrichment between the genes asssociated with the 657 non-responder sites and non-canonical AR target genes,[24] we used the 'phyper' function in R to perform a hypergeometric test with the two files and a 'universe' of genes taken from Ensembl genes with a geneID, n=40797.

To compare H3K27ac signal across various samples for our 657 non-responder H3K27ac regions of interest, we first downloaded public PDX mCRPC H3K27ac ChIP-seq data[18] (GSE130408) and additional H3K27ac data from primary prostate cancer patient tumors (GSE120738)[9] and aligned as above. In addition, we examined H3K27ac data in the same manner from in-house generated datasets from treatment naïve metastatic samples, non-responder metastatic samples (this study), and publicly available healthy and primary tumor tissue (GSE130408).[18] Visualizations of these data were generated with deepTools v2.0 computeMatrix followed by plotHeatmap of individual files and plotProfile as described above for binding data between groups.

Enrichment tests with gene sets using scRNA-seq clusters were performed in R (v4.1.2) using the GeneOverlap package (v1.30.0)[76] and visualized in ggplot2 (v3.4.0).[77] The average expression of these genes was calculated and plotted in public scRNA-seq from parental LNCaP cells and cells exposed to ENZA until resistance arose (RES-B[28,65]) using the Seurat package (v4.3.0)[78] in R (v4.1.2).

Read counts and fraction of reads in peaks (FRiP) were visualized using the ggplot2 (v2.3.3.0)[77] with Wilcoxon tests performed with ggpubr package v0.3.0[79] in R v3.5.0. To determine significant enrichment of our intervals with publicly available ChIP-seq data we queried our intervals against the CistromeDB transcription factor dataset[31] using the GIGGLE search function.[29] Briefly, the GIGGLE analysis is a genomics search engine that allows for the ranking of significance of genomic loci shared between query (non-responder regions) and a database of ChIP-seq regions. We used a database of prostate and prostate cancer ChIP-seq experiments (Table S3) specifically for analysis. A scatterplot of the median Enrichment score (combo_score) for each factor was generated using ggplot2 (v2.3.3.0)[77] in R v3.5.0.

For PDX-derived cell lines, raw paired-end PDX derived cell lines (cPDX LuCaP) ChIP-seq data were aligned to hg38 using BWA v0.7.17.[67] Our methods are available on GitHub (https://github.com/sebastian-gregoricchio/SPACCa). Briefly, aligned reads were filtered for mapping quality (MQ) > 20 using samtools v1.16.1.[68] Duplicate reads were marked using gatk (v4.3.0.0)[80] UmiAwareMarkDuplicatesWithMateCigar. Snapshots were generated as above. For analysis of experiments where there is an expected global reduction such as H3K27ac ChIP-seq with vorinostat, we used the package ChIPseqSpikeInFree (v1.2.4) with our MQ20 filtered bam files[81] to create normalized bigwigs or normalized as above with patient ChIP-seq data. Visualizations of these data were generated with deepTools v2.0 as mentioned above.

RNA sample processing and sequencing

For each experiment, 1×10^6 cPDX LuCaP cells were seeded in hormone deprived conditions (DCC) for 3 days after which they were treated with 1nM R1881 (PerkinElmer) for 6 hours or with vehicle control (DMSO, Fisher). RNA was isolated using the RNeasy Mini Kit (74106, Qiagen) following the manufacturer's instructions. Quality and amount of the total RNA was evaluated using a Nano chip (Agilent, Santa Clara, CA) in the 2100 Bioanalyzer. Samples of total RNA with a RIN greater than 8 underwent library preparation. Using the TruSeq Stranded mRNA sample preparation kit (Illumina Inc., San Diego, RS-122-2101/2) according to the manufacturer's instructions (Illumina, Document #1000000040498 v00). Briefly, strand-specific libraries were produced from polyadenylated RNA from total RNA using oligo-dT beads. After purification, the RNA was divided into fragments, primed, and then reverse transcribed using Actinomycin D and SuperScript II Reverse Transcriptase (Invitrogen, part # 18064-014). DNA Polymerase I and RNaseH were used to synthesize the second strand and digest the RNA template, substituting dTTP with dUTP. The resulting cDNA fragments were amplified using twelve rounds of PCR after being 3' end adenylated and ligated to IDT xGen UDI (10bp)-UMI(9bp) paired-end sequencing adapters (Integrated DNA Technologies, Inc., Coralville). The samples were pooled equimolarly into a multiplex sequencing pool after being examined on a 2100 Bioanalyzer with a 7500 chip (Agilent, Santa Clara, CA). 54 paired-end reads from the libraries were sequenced on a NovaSeq6000 with a Reagent Kit v1.5 (100 cycles) from Illumina Inc.

Following sequencing, HISAT2 (v2.1.0)[82] was used to align the data to the human reference genome hg38/GRCh38, and HTSeq count (v0.5.3)[83] was used to determine the number of reads per gene.

Publicly available single-cell RNA-seq (GSE168669) data was used to produce UMAP visualizations of LNCaP parental and LNCaP RES-B retaining cluster identities from Taavitsainen et al.[28] The genes proximal to the 657 non-responder H3K27ac sites were compiled into a gene set expression analysis to produce scores per cell with AddModuleScore function from Seurat (version 4.3.0). Previously identified single-cell clusters (clusters 0 to 12)[28] were used in the enrichment analysis to overlap genes proximal to the 657 non-responder H3K27ac sites.

siRNA proliferation assay and screen analysis

siRNAs were purchased from Dharmacon (Lafayette, CO, USA). Non-targeting siRNA and siPLK1 were applied as positive and negative controls. 5µl of 50nM siRNA pools were seeded in individual wells of a 96 well-plate. Cells were reverse transfected with 5µl 1%

Lipofectamine RNAiMAX Reagent (Invitrogen, Eindhoven, Netherlands) in Optimem (Thermofisher, Eindhoven, Netherlands) in 90μl culture medium. For LNCaP-Abl and LNCaP-16D, 10.000 cells were seeded per well, and 20.000 cells for LNCaP-Enz^{R} cells. Optimal experimental setup was determined for each cell line and after 7 (LNCaP-16D), 9 (LNCaP-Abl) and 10 (LNCaP-Enz^{R}) days, cell viability was determined using CellTiter-Blue and values were normalized over siControl. After incubating for 3 hours, viability was measured using a fluorescence reader (EnVision 2014).

The primary pooled siRNA and validation deconvolution screen were analysed with the following approach. Using the CellTiter-Blue measurements of the positive and negative controls, a z' factor was calculated per plate and plates with a z' factor < 0 were removed from the dataset. The data was then normalized using the Normalized percent inhibition as described previously.[91] After normalization, correlations between replicate plates were calculated and plates which did not correlate well with the other replicate plates, were removed. Over the replicates a mean value was calculated. Per condition a normalized distribution for mean values of the negative controls was approximated based on mean and SD value, and used to calculate for each pooled siRNA a p-value, which was corrected for multiple testing using the Benjamini-Hochberg method. From the primary screen of 4 pooled siRNAs per target (genes with median GIGGLE combo enrichment score >20, FOXA1, GATA2, NKX3-1, CREB1, HDAC3, TLE3, PIAS1, ASH2L, HOXB13, NR3C1, TOP1, AR, HDAC2, HNF4G, SUMO2) an initial selection was made of the siRNA pools that were a hit in at least two out of three cell lines, which produced a list of 11 hits. The 11 hits from the primary pooled screen were subsequently selected for a deconvolution validation screen, in which four individual siRNAs were tested separately. All targets with two individual siRNAs with among replicates a mean $\leq$ 0.7 and FDR $\leq$ 0.1, where considered validated hits. All calculation were done in R.

Expression levels per target gene in siRNA deconvolution experiments were assessed by means of qPCR analysis, using specific primer-pairs for ACTB (5'-CCTGGCACCCAGCACAAT-3', 5'-GGGCCGGACTCGTCATACT-3'), FOXA1 (FW 5'-GTGAAGATGGAA GGGCATGAA-3', REV 5'-CCTGAGTTCATGTTGCTGACC-3'), ASH2L (FW 5'-CTGACGTCTTGTATCACGTG-3', REV 5'-GCAT CTTTGGGAGAACATTTG-3'), GATA2 (FW 5'-GACAAGGACGGCGTCAAGTA-3', REV 5'-GGTGCCCATAGTAGCTAGGC-3') and HDAC3 (FW 5'-ACGGTGTCCTTCCACAAATACG-3', REV 5'-GGTGCTTGTAACTCTGGTCATC-3'). In brief, after siRNA transfection using the abovementioned protocol RNA was isolated using RNAGEM kit (MicroGEM), and quantified by Quant-iT^{TM} RiboGreen^{TM} RNA Assay Kit (Thermo Fisher Scientific), following quantification cDNA was synthesized using the SuperScript^{TM} III Reverse Transcriptase system (Thermo Fisher Scientific, USA) with random hexamer primers according to the instructions provided by manufacturers. Quantitative PCR (qPCR) was performed using the SensiMix^{TM} SYBR Kit (Bioline, UK) according to the manufacturer's instructions on a QuantStudio^{TM} 6 Flex System (Thermo Fisher Scientific, USA). All data was firstly normalized over ACTB expression, and then over the siControl values. For all primer pairs, 2 biological replicates with 2 technical replicates each were analyzed.

Response to castration in PDX models

Responses to castration were also fully described previously.[27] The doubling time was estimated using exponential (Malthusian) growth model. If only one value was available, doubling time was not computed. For samples with a negative doubling time, the value was re-normalized to the mean value of the corresponding control model yielding a positive value. Significant differences between classes determined by one-way ANOVA followed by post-hoc Tukey honest significant difference (HSD) test. Visualization was carried out in R using ggplot (v3.3.6).[77]

Drug synergy assessment in cell lines and explants

For cell line studies, 500 LNCaP or LNCaP-16D cells were seeded in a 384-well plate, and treated with various concentrations of ENZA (MedChemExpress, Monmouth Junction NJ, USA) and vorinostat (kindly provided by Rene Bernards, NKI). Five days later, the CellTiter Glo assay (Promega Benelux BV, Leiden, Netherlands) was performed according to the manufacturer's instruction. All the assays were performed in biological quadruplicates (n=4).

For explant studies, subcutaneous tumors were harvested and dissociated using the Miltenyi gentleMACS system with a Human Tumor dissociation kit (Miltenyi Corp). Cells were seeded in clear bottom white -walled flat bottom 96-well plates (20,000 cells per well) in RPMI and 10% FBS. ENZA (MedChem Express) and vorinostat (MedChem Express) 10mM in DMSO and diluted with RPMI to indicated concentrations. Effects of the treatments were evaluated after 5 days using CellTiter-Glo (Promega).

Synergy assessment analyses for all the conditions (single and combination) were normalized to non-treated condition (set at 100). SynergyFinder 2.0[84] was used to evaluate and plot synergistic potential using highest-single agent (HSA) synergy reference model. Response of the two cell lines to single agent vorinostat was also investigated and plotted using the normalized viability in full media (FBS) and area under the curve (AUC) method.

PDX derived cell line proliferation assays

The cPDX LuCaP 189.4 cells were seeded in a 384 well plate at a density of 2.2×10^3 cells or 3.1×10^3 cells per well in FBS conditions. After seeding, the cells were treated with 1 μM vorinostat (MedChemExpress), 10 μM BRD3308 (MedChemExpress) or 10 μM RGFP966 (MedChemExpress) either as a single treatment or in combination with 10 μM ENZA (MedChemExpress) using the HP D300e Digital Dispenser. The cells were imaged every 4 hours using an IncuCyte ZOOM Live-cell Analysis System. Following the experiment, the confluency percentage of a well was assessed using the IncuCyte Zoom software. Each condition shown is performed in biological triplicates with all 6 technical replicates and the results are shown as non-normalized well confluency (%) ± SEM.

Western blotting

The cPDX LuCaP 189.4 and 35 cells were plated in a 6-well plate with a cell density of 3×10^5 cells/well in FBS conditions. After seeding, the cells were treated with the given concentrations of vorinostat (MedChemExpress), BRD3308 (MedChemExpress) and RGFP966 (MedChemExpress) as a single treatment for either 2 or 6 hours. Upon treatment, the total proteins were isolated using a 2x Laemmli lysis buffer (120 mM Tris, 20% glycerol, 4% SDS) supplemented with EDTA-free protease inhibitor cocktail (Roche). Whole cell lysates were sonicated for 10 cycles with the settings 1 s off/1 s off, 20% amplitude. Quantification of protein amounts was done by BCA assay (Thermo Fisher Scientific). Per sample, 30 μg of protein was resolved by NuPAGE Bis-Tris 4-12% gels (Life Technologies) in MOPS running buffer and transferred to a 0.22 μm nitrocellulose membrane (Santa Cruz). Transfer quality was assessed using Ponceau Red staining before blocking with 3% BSA followed by antibody incubation. Immunoblotting was performed with antibodies directed against HDAC3 (ab137704, Abcam), H3K27ac (39133, Active Motif), AR (Millipore, 06-6890), FOXA1 (Seven Hills Bioreagents, WMAB-2F83) and HSP90 (Santa Cruz, sc-7947). Blots were incubated overnight at 4°C with designated primary antibodies at 1:1000, followed by incubation with fluorescent-tagged secondary antibodies donkey-α-rabbit (LI-COR Biosciences, 926-32213) and donkey-α-mouse (Li-COR, 926-68072) at 1:10.000. Detection was done with the Li-COR Odyssey CLx Imaging system (Li-COR Biosciences) and processed with Image Studio Lite v5.5 (Li-COR Biosciences).

In vivo PDX derived cell line injection and monitoring of tumor growth

For tumor generation, we injected 2 million cPDX LuCaP 189.4 cells in BME (Bio-Techne, 3536-005-02) into the flank of NOD-Scid IL2Rag null (Jackson Laboratory, USA) male mice. Mice were weighed and monitored three times a week after injection. Tumor volume was measured with calipers three times weekly. Endpoint was reached when the tumor reached 1500mm^3 or mice were sacrificed for humane reasons. Once tumors reached established size of 100mm^3, 10 mice were randomized to 4 treatment groups: 1) Vehicle arm: ENZA vehicle control oral daily for 4 weeks (1% carboxymethylcellulose sodium salt, 0.1% Tween-80 in water) + Vorinostat vehicle control intraperitoneal injection daily for 4 weeks (1:1:8, DMSO, CreEl, Water) after tumor becomes 100mm^3 (n=10, biological replicates (also other treatments), 2) ENZA arm: ENZA 8mg/kg in vehicle (1% carboxymethylcellulose sodium salt, 0.1% Tween-80 in water) through oral gavage on a daily basis for 4 weeks after tumor becomes 100mm^3 (n=10), 3) Vorinostat arm: Vorinostat 80mg/kg in vehicle (1:1:8, DMSO, CreEl, Water) through intraperitoneal injection on a daily basis for 4 weeks after the tumor becomes 100mm^3 (n=10), 4) Combination arm: ENZA 8mg/kg in vehicle (1% carboxymethylcellulose sodium salt, 0.1% Tween-80 in water) through oral gavage on a daily basis for 4 weeks after tumor becomes 100mm^3. Vorinostat 80mg/kg in vehicle (1:1:8, DMSO, CreEl, Water) through intraperitoneal injection on a daily basis for 4 weeks after the tumor becomes 100mm^3 (n=9).

Statistical analysis of tumor growth curves depicted in Figure 5C were performed in R using a linear mixed effects model function, 'lme' with tumor volume and treatment day as variables.[92] The model included a random effect for each animal, as well as fixed effects for time and the interaction between time and treatment. The latter is the variable of interest, indicating evidence for different tumor growth rates between animals in the control (vehicle) and in each of the treatment groups (group 1 vehicle, group 2 ENZA, group 3 vorinostat, or group 4 combination).

QUANTIFICATION AND STATISTICAL ANALYSIS

R computing software was used for statistical analysis. Statistical details of experiments can be found in figure legends and text. Significance is considered as $p < 0.05$.

ADDITIONAL RESOURCES

Public PDX mCRPC, healthy prostate and primary prostate tumor H3K27ac data from GEO: GSE130408. Additional public primary prostate cancer tumor H3K27ac data from GEO: GSE120738. Additional public scRNA-seq data from LNCaP cells and LNCaP RES-B cells from GEO: GSE130534 and GEO: GSE168669, respectively.